



2 Evaluation of space-based constraints on global nitrogen oxide 3 emissions with regional aircraft measurements over and downwind of 4 eastern North America

5 Randall V. Martin,^{1,2} Christopher E. Sioris,³ Kelly Chance,³ Thomas B. Ryerson,⁴
6 Timothy H. Bertram,⁵ Paul J. Wooldridge,⁵ Ronald C. Cohen,⁵ J. Andy Neuman,^{6,7}
7 Aaron Swanson,^{6,8,9} and Frank M. Flocke¹⁰

8 Received 17 September 2005; revised 20 April 2006; accepted 1 May 2006; published XX Month 2006.

9 [1] We retrieve tropospheric nitrogen dioxide (NO₂) columns for May 2004 to April 2005
10 from the SCIAMACHY satellite instrument to derive top-down emissions of nitrogen
11 oxides (NO_x = NO + NO₂) via inverse modeling with a global chemical transport model
12 (GEOS-Chem). Simulated NO₂ vertical profiles used in the retrieval are evaluated with
13 airborne measurements over and downwind of North America (ICARTT); a northern
14 midlatitude lightning source of 1.6 Tg N yr⁻¹ minimizes bias in the retrieval. Retrieved
15 NO₂ columns are validated ($r^2 = 0.60$, slope = 0.82) with coincident airborne in situ
16 measurements. The top-down emissions are combined with a priori information from a
17 bottom-up emission inventory with error weighting to achieve an improved a posteriori
18 estimate of the global distribution of surface NO_x emissions. Our a posteriori NO_x
19 emission inventory for land surface NO_x emissions (46.1 Tg N yr⁻¹) is 22% larger than
20 the GEIA-based a priori bottom-up inventory for 1998, a difference that reflects rising
21 anthropogenic emissions, especially from East Asia. A posteriori NO_x emissions for East
22 Asia (9.8 Tg N yr⁻¹) exceed those from other continents. The a posteriori inventory
23 improves the GEOS-Chem simulation of NO_x, peroxyacetyl nitrate, and nitric acid with
24 respect to airborne in situ measurements over and downwind of New York City. The a
25 posteriori is 7% larger than the EDGAR 3.2FT2000 global inventory, 3% larger than the
26 NEI99 inventory for the United States, and 68% larger than a regional inventory for 2000
27 for eastern Asia. SCIAMACHY NO₂ columns over the North Atlantic show a weak plume
28 from lightning NO_x.

29 **Citation:** Martin, R. V., C. E. Sioris, K. Chance, T. B. Ryerson, T. H. Bertram, P. J. Wooldridge, R. C. Cohen, J. A. Neuman,
30 A. Swanson, and F. M. Flocke (2006), Evaluation of space-based constraints on global nitrogen oxide emissions with regional aircraft
31 measurements over and downwind of eastern North America, *J. Geophys. Res.*, *111*, XXXXXX, doi:10.1029/2005JD006680.

33 1. Introduction

34 [2] Nitrogen oxide radicals (NO_x ≡ NO + NO₂) largely
35 control tropospheric ozone production [Kasibhatla *et al.*,
36 1991; Penner *et al.*, 1991; Murphy *et al.*, 1993; Jacob *et al.*,
37 1996], oxidize in the atmosphere to form nitric acid (HNO₃)
38 that affects cloud properties [Nenes *et al.*, 2002] and
39 contributes to aerosol formation [Adams *et al.*, 2001], and
40 subsequently deposit to the surface with implications for
41 marine [Michaels *et al.*, 1996] and terrestrial [Holland and

Lamarque, 1997] ecosystems. Anthropogenic activity has 42
increased global NO_x emissions by a factor of 3–6 since 43
preindustrial times [Prather *et al.*, 2001]. Assessments of 44
the implications of NO_x emissions usually are based on 45
“bottom-up” inventories as determined by aggregating 46
information about sources from diverse sources such as fuel 47
and land use statistics, in-tunnel measurements of NO_x 48
emission ratios, agricultural data, and estimates of burned 49
areas. “Top-down” information from space-based observa- 50

¹Department of Physics and Atmospheric Science, Dalhousie University, Halifax, Nova Scotia, Canada.

²Also at Harvard-Smithsonian Center for Astrophysics, Cambridge, Massachusetts, USA.

³Harvard-Smithsonian Center for Astrophysics, Cambridge, Massachusetts, USA.

⁴Chemical Sciences Division, Earth System Research Laboratory, NOAA, Boulder, Colorado, USA.

⁵Department of Chemistry, University of California, Berkeley, Berkeley, California, USA.

⁶Cooperative Institute for Research in Atmospheric Sciences, Boulder, Colorado, USA.

⁷Also at Chemical Sciences Division, Earth System Research Laboratory, NOAA, Boulder, Colorado, USA.

⁸Formerly at Chemical Sciences Division, Earth System Research Laboratory, NOAA, Boulder, Colorado, USA.

⁹Formerly at Atmospheric Chemistry Division, National Center for Atmospheric Research, Boulder, Colorado, USA.

¹⁰Atmospheric Chemistry Division, National Center for Atmospheric Research, Boulder, Colorado, USA.

tions of NO₂ columns provides additional constraints that could yield an improved NO_x emission inventory and an improved representation of processes affecting NO_x.

[3] Bottom-up NO_x emission inventories for a specific year quickly could become outdated in a rapidly industrializing economy. An increase in global NO_x emissions of more than 50% is expected over 2000–2020 [Intergovernmental Panel on Climate Change, 2001] with most of this increase from Asia. Rising Asian emissions may have implications for radiative forcing by tropospheric ozone [Berntsen et al., 1997; Brasseur et al., 1998; Wild et al., 2001] and for surface air quality throughout the Northern Hemisphere [Jacob et al., 1999; Fiore et al., 2002; Lelieveld et al., 2002; Derwent et al., 2004]. Global numerical models rely on current information for simulation of atmospheric composition and for climate change assessments. Space-based measurements provide timely information that could be used to more accurately reflect current emissions.

[4] The SCanning Imaging Absorption spectroMeter for Atmospheric CHartography (SCIAMACHY) instrument onboard the ENVISAT satellite provides the capability for global measurement of atmospheric NO₂ columns through observation of global backscatter [Bovensmann et al., 1999]. The satellite was launched in March 2002 into a sun-synchronous orbit, crossing the equator at 1000 local time in the descending node. The SCIAMACHY instrument observes the atmosphere in the nadir view with a typical surface spatial resolution of 30 km along track by 60 km across track. Global coverage is achieved every 6 days. An advantage of SCIAMACHY over the earlier Global Ozone Monitoring Experiment (GOME) satellite instrument [European Space Agency, 1995; Burrows et al., 1999] is that the surface spatial resolution of SCIAMACHY is seven times higher than that of GOME. The higher resolution is expected to reduce the retrieval error by reducing subpixel variation, especially from clouds. The close relationship between tropospheric NO₂ columns and land surface NO_x emissions has been previously demonstrated with GOME observations [Leue et al., 2001; Beirle et al., 2003; Martin et al., 2003b; Jaeglé et al., 2005; Müller and Stavrou, 2005]. Here we apply the higher resolution SCIAMACHY measurements to produce an improved NO_x emission inventory.

[5] A prerequisite for this analysis is an understanding of the accuracy of the SCIAMACHY retrieval, and of the emission inventory. We focus on the summer of 2004 during which the International Consortium for Atmospheric Research on Transport and Transformation (ICARTT) aircraft campaign occurred over eastern North America and the North Atlantic Ocean. Section 2 describes the numerical model used in our analysis. In section 3 we retrieve tropospheric NO₂ columns from SCIAMACHY as our top-down constraint and validate the retrieval with airborne measurements of NO₂. Section 4 presents the a posteriori NO_x emission inventory and evaluates it with airborne measurements. The a posteriori is compared with independent bottom-up inventories in section 5.

2. Global Chemical Transport Model

[6] We use the GEOS-Chem global 3-D model of atmospheric composition to provide NO₂ profiles to constrain the

SCIAMACHY retrieval as described in section 3.1, to conduct a simple inversion to infer NO_x emissions from the observed NO₂ columns as described in section 4.1, and to serve as an intermediary to compare the a priori and a posteriori NO_x emission inventories with airborne in situ observations as described in section 4.3. The simulation is driven by assimilated meteorological data from the Goddard Earth Observing System (GEOS-4) at the NASA Global Modeling and Assimilation Office (GMAO). The data have 6-hour temporal resolution (3-hour resolution for surface variables and mixing depths) and 1° × 1.25° horizontal resolution. There are 55 hybrid eta vertical levels, extending from the surface to 0.01 hPa. The lowest 2 km is resolved by five layers with midpoints at 60, 250, 620, 1200, and 1990 m altitude for a column based at sea level. We use version 7-01-02 of GEOS-Chem (www-as.harvard.edu/chemistry/trop/geos) at 2° × 2.5° horizontal resolution with updated midlatitude lightning NO_x emissions as described below.

[7] The GEOS-Chem model includes a detailed simulation of tropospheric ozone-NO_x-hydrocarbon chemistry as well as of aerosols and their precursors using 41 tracers, ~90 species, and ~300 reactions. The ozone-NO_x-hydrocarbon simulation was first described by Bey et al. [2001] with updates by Fiore et al. [2002] and Martin et al. [2002a, 2003a]. The model presently includes sulfate, nitrate, ammonium, black carbon, organic carbon, mineral dust, and sea salt [Park et al., 2003, 2004; Alexander et al., 2005; Park et al., 2005]. The aerosol and gaseous simulations are coupled through formation of sulfate and nitrate, HNO₃(g)/NO₃⁻ partitioning of total inorganic nitrate, heterogeneous chemistry on aerosols [Jacob, 2000; Evans and Jacob, 2005], and aerosol effects on photolysis rates [Martin et al., 2003a]. Simulation of wet and dry deposition follows the schemes developed by Bey et al. [2001]; extension to moderately soluble gases with low retention efficiencies upon cloud freezing is as described by Park et al. [2004].

[8] Table 1 contains the annual global NO_x emissions in GEOS-Chem for all sources. Anthropogenic NO_x emissions are from the Global Emission Inventory Activity (GEIA) [Benkovitz et al., 1996] and scaled by country based on energy statistics to 1998 (the last year of available statistics) as described by Bey et al. [2001]. Time-of-day and day-of-the-week variation are based on work of Environmental Protection Agency [1989] as described by Jacob et al. [1993]. Soil NO_x emissions are computed using a modified version of the algorithm of Yienger and Levy [1995] with the canopy reduction factors described by Wang et al. [1998]. The climatological biomass burning inventory is seasonally varying and is based on satellite observations of fires over 1996–2000 from the Along Track Scanning Radiometer (ATSR) as derived by Duncan et al. [2003]. Emissions of lightning NO_x are linked to deep convection following the parameterization of Price and Rind [1992] with vertical profiles from Pickering et al. [1998] as implemented by Wang et al. [1998]. The magnitude of the tropical source is constrained to reproduce ozone observations as described by Martin et al. [2002a]. Northern midlatitude lightning NO_x emissions are increased here by a factor of 4 to 1.6 Tg N yr⁻¹ for consistency with aircraft observations as described in section 3.2. The resulting ratio of midlatitude to tropical lightning NO_x emissions is more

t1.1 **Table 1.** A Priori Annual Global GEOS-Chem NO_x Emissions

t1.2	Source	Emissions, Tg N
t1.3	Fossil fuel combustion ^a	23.3 (11.5) ^b
t1.4	Lightning	7.1 (4.2)
t1.5	Biomass burning	6.0 (3.7)
t1.6	Soils	7.1 (3.5)
t1.7	Biofuels	2.2 (1.1)
t1.8	Aircraft	0.5 (0.26)
t1.9	Stratosphere	0.1 ^c (0.05)

t1.10 ^aFossil fuel emissions are based on GEIA and scaled to 1998.t1.11 ^bValues for May–October are given in parentheses.t1.12 ^cThe cross-tropopause NO_y flux is 0.5 Tg N yr⁻¹ (including 0.1 Tg N yr⁻¹ as NO_x and 0.4 Tg N yr⁻¹ as HNO₃).

173 consistent with the ratio of midlatitude to tropical lightning
 174 flashes of 22% determined by *Christian et al.* [2003]
 175 using space-based observations from the Optical Transient
 176 Detector.

177 3. SCIAMACHY Tropospheric NO₂ Retrieval

178 3.1. Retrieval Algorithm

179 [9] Our retrieval of tropospheric NO₂ columns presented
 180 here is based on the algorithms of *Martin et al.* [2002b,
 181 2003b]. We focus on May–October 2004, a time period that
 182 brackets the ICARTT campaign, but extend the retrieval to
 183 April 2005 to span an entire year. Level-1 SCIAMACHY
 184 data for January–April 2004 were not available to us at the
 185 time.

186 [10] Following *Chance* [1998] and *Martin et al.* [2002b]
 187 we determine total slant columns of NO₂ by directly fitting
 188 backscattered radiance spectra observed by SCIAMACHY.
 189 The spectral fit is optimized for SCIAMACHY over the
 190 wavelength region 429–452 nm using measured reference
 191 spectra for NO₂ at 243 K [*Bogumil et al.*, 2003], ozone at
 192 223K [*Bogumil et al.*, 2003], H₂O at 296 K [*Rothman et al.*,
 193 1998], O₂-O₂ at 296 K [*Greenblatt et al.*, 1990], and the
 194 Ring effect [*Chance and Spurr*, 1997]. The solar spectra for
 195 each orbit are from the elevation scan mirror on the
 196 SCIAMACHY instrument. We find no evidence of a dif-
 197 fuser plate artifact [*Richter and Wagner*, 2001; *Martin et al.*,
 198 2002b] that complicated retrievals of NO₂ from GOME.
 199 The stratospheric column and instrument biases are re-
 200 moved by assuming that NO₂ over the central Pacific is
 201 mainly stratospheric, subtracting the corresponding columns
 202 from the ensemble of SCIAMACHY observations for the
 203 appropriate latitude and month, and correcting the result for
 204 the small amount of tropospheric NO₂ over the Pacific. The
 205 stratospheric column is taken to be zonally invariant; this
 206 assumption does not cause significant error in summer
 207 [*Martin et al.*, 2002b], but is questionable at high latitudes
 208 in other seasons owing to dynamical variability [*Boersma et*
 209 *al.*, 2004].

210 [11] We apply the air mass factor (AMF) formulation of
 211 *Palmer et al.* [2001] to convert the resulting tropospheric
 212 slant columns into vertical columns. This formulation
 213 computes the AMF as the integral over the tropospheric
 214 column of the relative vertical distribution of NO₂ (shape
 215 factor) weighted by the local sensitivity to NO₂ of the solar
 216 radiation backscattered to space (scattering weights). The
 217 temperature dependence of the NO₂ cross section is
 218 accounted for using local GEOS-4 temperature profiles for

every SCIAMACHY scene. The shape factor for every 219
 SCIAMACHY scene is specified from a GEOS-Chem 220
 model simulation of that scene, while the scattering weights 221
 are calculated from the Linearized Discrete Ordinate Radi- 222
 ative Transfer (LIDORT) model [*Spurr et al.*, 2001; *Spurr*, 223
 2002]. Prior evaluation of the NO₂ shape factor with in situ 224
 airborne measurements in the lower troposphere over the 225
 southeast United States found agreement to within 20%; 226
 differences would affect the retrieved NO₂ columns by only 227
 a few percent [*Martin et al.*, 2004]. Monthly varying surface 228
 reflectivity fields are from *Koелеmeijer et al.* [2003]. Our 229
 aerosol correction uses daily local aerosol profiles from the 230
 GEOS-Chem simulation for that scene as described by 231
Martin et al. [2003b]. 232

[12] Our cloud correction in the AMF uses cloud top 233
 pressure and cloud fraction information from the 234
 Fast Retrieval Scheme for Cloud Observables (FRESCO) 235
 [*Koелеmeijer et al.*, 2002] algorithm. For consistency with 236
 FRESCO, clouds are treated as Lambertian surfaces here 237
 rather than as a collection of Mie scatterers as was possible 238
 in our GOME retrieval [*Martin et al.*, 2002b]. We exclude 239
 scenes in which the cloud radiance fraction is more than 240
 50%; that is, more than half of the backscattered intensity is 241
 from the cloudy-sky fraction of the scene as determined 242
 from the radiative transfer calculation constrained with the 243
 local cloud information. 244

[13] *Martin et al.* [2002b, 2003b] and *Boersma et al.* 245
 [2004] estimated that the total uncertainty in the GOME 246
 retrieval of tropospheric NO₂ columns over continental 247
 source regions is largely determined by the AMF calcula- 248
 tion due primarily to surface reflectivity, clouds, aerosols, 249
 and the trace gas profile. The uncertainty in each measure- 250
 ment exhibits large spatial variation [*Boersma et al.*, 2004]. 251
 The higher spatial resolution of SCIAMACHY over GOME 252
 is expected to reduce uncertainty in the AMF calculation 253
 due to reduction in subpixel variability, especially from 254
 clouds. However, we conservatively adopt the same uncer- 255
 tainty estimate in the AMF as with GOME owing to 256
 additional concern about the treatment of clouds as Lam- 257
 bertian surfaces in the SCIAMACHY AMF calculation. We 258
 estimate the typical 1-sigma uncertainty for each 259
 SCIAMACHY measurement is 40% due to the AMF plus 260
 an absolute component of 1×10^{15} molecules cm⁻² from 261
 spectral fitting and subtraction of the stratospheric NO₂ 262
 column. Our estimate for the monthly mean uncertainty is 263
 $\pm(5 \times 10^{14}$ molecules cm⁻² + 30%) which could include 264
 systematic errors. 265

266 3.2. Evaluation of NO₂ Profiles Used in the Retrieval; 267 Sensitivity to Lightning

[14] We validate our retrieval using coincident airborne in 268
 situ measurements as part of the ICARTT campaign. 269
 Figure 1 shows the flight tracks of the NASA DC-8 and 270
 NOAA WP-3D aircraft which spanned conditions from 271
 remote marine to highly polluted. The DC-8 sampled more 272
 remote regions than the WP-3D. NO₂ was measured on the 273
 DC-8 by laser induced fluorescence [*Thornton et al.*, 2000] 274
 and on the WP-3D by photolysis of NO₂ and chemilumi- 275
 nescence detection of the product NO [*Ryerson et al.*, 276
 2003]. 277

[15] As discussed above, independent information on the 278
 relative NO₂ vertical profile is necessary for determination 279

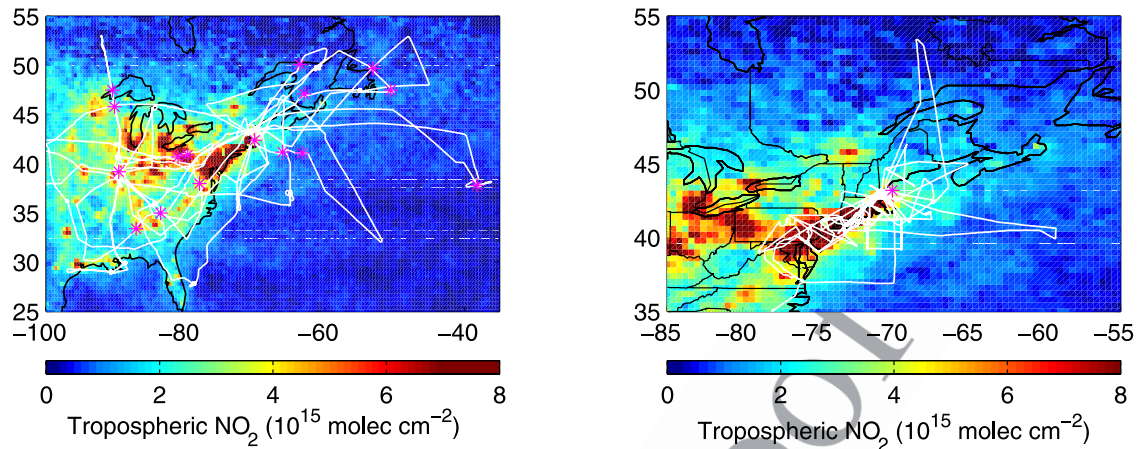


Figure 1. Tropospheric NO₂ columns retrieved from the SCIAMACHY satellite instrument for May–October 2004. White lines show flight tracks of the (left) DC-8 and (right) WP-3D aircraft. Magenta stars indicate the location of coincident aircraft and SCIAMACHY measurements used for validation.

280 of column abundance from SCIAMACHY. Figure 2 compares campaign-average profiles of NO₂ measured from
 281 aircraft with those calculated with the GEOS-Chem model.
 282 Here and elsewhere, model results are sampled along the
 283 flight tracks at the measurement time. Observations are
 284 averaged over model grid boxes. The aircraft and model
 285 profiles are generally consistent in the lower troposphere.
 286 However, the standard simulation with 0.4 Tg N yr⁻¹ of
 287 lightning from northern midlatitudes (north of 30°N) under-
 288 estimates NO₂ in the upper troposphere by 100 pptv. The
 289 AMFs calculated with the simulated profiles are lower than
 290 the AMFs calculated from the campaign-average in situ
 291 DC-8 profiles by 12% over land and 9% over ocean. We
 292 find no bias in the comparison of measured and simulated
 293 profiles of CO, providing evidence that the upper tropo-
 294 spheric bias in NO₂ is indeed from lightning and not
 295 convection. R. Hudman et al. (A multi-platform analysis
 296 of the North American reactive nitrogen budget during the
 297 ICARTT summer intensive, manuscript in preparation,
 298

2006) (hereinafter referred to as Hudman et al., manuscript
 299 in preparation, 2006) evaluated the GEOS-Chem simulation
 300 with in situ measurements of CO₂ and NO_y from the
 301 DC-8 and find little evidence for a model underestimate
 302 in aircraft NO_x emissions. 303

[16] We conduct an additional simulation with enhanced
 304 northern midlatitude lightning NO_x emissions (1.6 Tg N
 305 yr⁻¹). Tropical lightning NO_x emissions remain unchanged. 306
 Figure 2 shows that the simulation with enhanced midlati-
 307 tude lightning reduces the model underestimate of NO₂ in
 308 the upper troposphere by more than a factor of 2, but
 309 introduces a positive bias of 20 pptv in the middle tropo-
 310 sphere. The remaining bias in the model vertical placement
 311 of lightning NO_x may be explained by low cloud top heights
 312 in the GEOS-4 meteorological fields (Hudman et al.,
 313 manuscript in preparation, 2006), or by an underestimate
 314 in NO_x emissions from intracloud discharges; Fehr et al.
 315 [2004] and DeCaria et al. [2005] compared aircraft NO_x
 316 measurements with a three-dimensional cloud model and 317

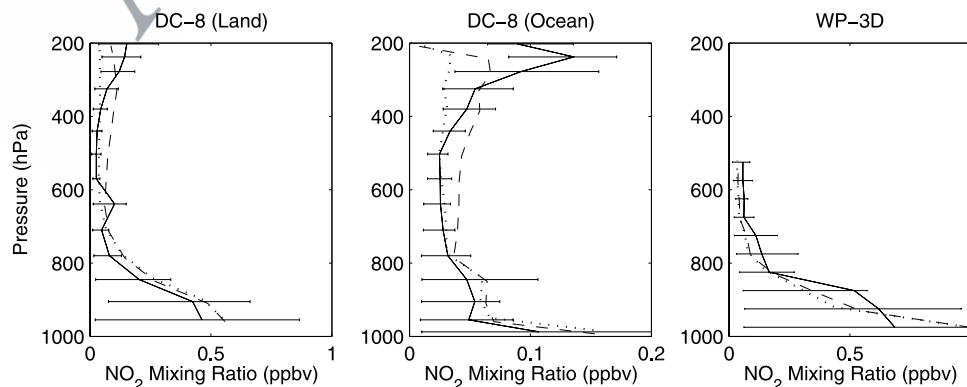


Figure 2. Vertical profiles of NO₂ over eastern North America averaged over the entire ICARTT campaign. In situ measurements (solid lines) are compared with a GEOS-Chem simulation with 1.6 Tg N yr⁻¹ from northern midlatitude lightning (dashed lines) and a sensitivity simulation with 0.4 Tg N yr⁻¹ from northern midlatitudes lightning (dotted lines). Horizontal bars represent 17th and 83rd percentiles of the measurements.

t2.1 **Table 2.** Characteristics of Measurements Used for Validation

t2.2	Date	Latitude, deg	Longitude, deg	SCIAMACHY Time, UTC	Aircraft Time, UTC	Aircraft Altitude, km
t2.3	8 July	38.0	-78.0 ^a	1515	1946–2011	0.4–3.2
t2.4	10 July	40.7	-81.1	1558	1532–1547	0.7–5.8
t2.5	10 July	40.9	-79.7	1558	1547–1621	0.7–10.6
t2.6	10 July	35.0	-83.6	1600	1822–1859	0.9–11.4
t2.7	10 July	33.4	-87.1	1600	1911–1939	0.4–11.3
t2.8	12 July	39.2	-89.6	1636	1509–1528	0.7–6.4
t2.9	12 July	45.8	-90.2	1634	1622–1656	0.7–10.5
t2.10	15 July	47.5	-90.5	1639	1456–1520	0.5–9.7
t2.11	18 July	47.1	-63.0	1505	1441–1514	0.3–10.0
t2.12	22 July	50.1	-63.6	1438	1840–1911	0.5–9.2
t2.13	28 July	37.8	-38.2	1312	1658–1728	0.3–9.0
t2.14	31 July	42.4	-70.1	1457	1459–1514	0.4–6.8
t2.15	31 July	41.2	-66.1	1457	1600–1632	0.3–9.4
t2.16	31 July	41.1	-63.3	1457	1642–1705	0.3–9.1
t2.17	31 July	43.2	-70.1 ^b	1457	2125–2136	0.04–3.6
t2.18	2 Aug	49.7	-53.1	1352	1740–1755	0.3–6.6
t2.19	2 Aug	47.5	-50.6	1352	1811–1831	0.3–7.9

t2.20 ^aLocations correspond to the center of the SCIAMACHY pixel.t2.21 ^bAirborne measurements at this location are from the WP-3D aircraft. All other locations were sampled from the DC-8 aircraft.

318 concluded that intracloud lightning discharges are more
 319 energetic than derived by *Price et al.* [1997] as implemented
 320 in GEOS-Chem using profiles from *Pickering et al.* [1998].
 321 The biases in the AMF calculated with the simulated
 322 profiles, versus the AMF calculated from the campaign-
 323 averaged in situ profiles, are reduced to 1% over land
 324 and 5% over ocean using the simulation with enhanced
 325 lightning. We use the simulation with 1.6 Tg N yr⁻¹
 326 from northern midlatitude lightning in our SCIAMACHY
 327 retrieval.

3.3. Validation of Retrieved NO₂ Columns With in Situ Measurements

330 [17] Table 2 contains the characteristics of the satellite
 331 and airborne measurements used here for validation. Several
 332 dedicated aircraft spirals were conducted during
 333 SCIAMACHY overpasses for validation purposes. Addi-
 334 tional comparisons of opportunity also are considered if
 335 they satisfy the following coincidence criteria. Daytime
 336 measurements must occur within a SCIAMACHY scene
 337 on the date of observation; the two measurements were
 338 usually within hours of each other. Many WP-3D measure-
 339 ments were at night and excluded from the comparison. The
 340 in situ measurements must sample the lower troposphere
 341 below 1 km and up to at least 3 km. Over regions with
 342 enhanced NO₂ (>3 × 10¹⁵ molecules cm⁻²), which likely
 343 have spatially heterogeneous surface sources, in situ meas-
 344 urements must be taken within 15 km of the center of the
 345 SCIAMACHY pixel. Nearly 20 coincident measurements
 346 are found, providing an unprecedented opportunity to
 347 validate SCIAMACHY retrievals.

348 [18] Partial columns are calculated from the airborne
 349 measurements by integrating the average NO₂ number
 350 density from the surface to the highest measurement alti-
 351 tude. The vertical step size is 700 m for the WP-3D
 352 measurements and 1000 m for the DC-8. The larger step
 353 size for the DC-8 accommodates its infrequent altitude
 354 below 700 m. The partial tropospheric column above the
 355 highest measurement altitude of an individual profile is
 356 determined by integrating a mean profile determined from

the average NO₂ measured on all DC-8 flights over eastern
 North America and the North Atlantic Ocean that were
 coincident with a SCIAMACHY measurement.

[19] Figure 3 compares tropospheric NO₂ columns re-
 trieval from SCIAMACHY with those determined with in
 situ measurements. The geometric mean in situ to
 SCIAMACHY ratio m is 0.82 with a geometric standard
 deviation σ of 1.69 (i.e., 67% of the values are between m/σ
 and $m\sigma$). The coefficient of determination, r^2 , is 0.60. The
 slope of the reduced-major axis regression line is 0.82. The
 two measurement techniques are consistent within their
 uncertainty. However, the comparison exhibits modest scatter
 that likely is related to incomplete sampling of the entire
 vertical column and of the potentially heterogeneous lower
 mixed layer. Columns calculated from in situ measurements
 tend to be lower than those determined from SCIAMACHY
 over remote regions, and higher over regions with enhanced
 NO₂. A similar degree of consistency was found during a
 previous SCIAMACHY validation exercise over southern
 Europe [*Heue et al.*, 2005].

3.4. Retrieved NO₂ Columns

[20] Figure 4 shows tropospheric NO₂ vertical columns
 retrieved from SCIAMACHY for May 2004 to April 2005.
 Pronounced enhancements are apparent over major indus-
 trial and metropolitan areas. The high spatial heterogeneity
 in regions with distinct sources, such as the southwestern
 United States and the Middle East, provides empirical
 evidence of the short NO_x lifetime that facilitates mapping
 of NO₂ columns onto NO_x emissions. Moderate enhance-
 ments are found in central Africa from biomass burning
 [*Richter and Burrows*, 2002]. An enhancement of compa-
 rable magnitude is observed over northern equatorial Africa
 with a maximum at the beginning of the rainy season in
 early June that *Jaeglé et al.* [2004] attributed to rain-induced
 soil NO_x emissions. There are weak enhancements along
 ocean ship tracks near Kuala Lumpur [*Beirle et al.*, 2004b;
Richter et al., 2004].

[21] Tropospheric NO₂ columns are more sensitive to
 NO_x in the lower troposphere than in the upper troposphere

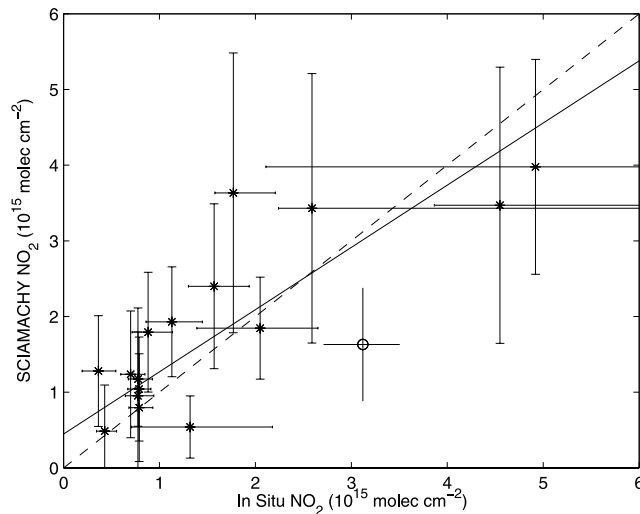


Figure 3. Comparison of coincident NO₂ columns retrieved from SCIAMACHY with those determined from in situ measurements on the WP-3D (circle) and DC-8 (stars) aircraft. Vertical lines indicate the SCIAMACHY retrieval uncertainty. Horizontal lines are determined by summing vertically in quadrature the difference between the mean and the 17th and 83rd percentiles of in situ measurements. The dashed line represents the $y = x$ line. The solid line was calculated with reduced major-axis linear regression [Hirsch and Gilroy, 1984].

[Martin et al., 2002b]. This sensitivity is due largely to the 396 large decrease in the NO₂/NO_x ratio with increasing altitude 397 that is driven the temperature dependence of the NO + O₃ 398 reaction. However, there is mounting evidence of a light- 399 ning NO_x signal in GOME observations of tropospheric 400 NO₂ [Richter and Burrows, 2002; Edwards et al., 2003; 401 Beirle et al., 2004a, 2005; Boersma et al., 2005; Choi et al., 402 2005]. Figure 2 indicates that North American lightning 403 NO_x emissions make a larger relative contribution to the 404 mean NO₂ column over ocean than over land. Close 405 inspection of our SCIAMACHY NO₂ columns during 406 summer reveals a weak plume from North American light- 407 ning NO_x emissions that extends across the North Atlantic 408 Ocean to Europe. 409

[22] Figure 5 shows retrieved and simulated NO₂ col- 410 umns over the North Atlantic Ocean during May–October 411 2004. The SCIAMACHY NO₂ columns are near the detec- 412 tion limit of 5×10^{14} molecules cm⁻². The spatial extent of 413 the NO₂ plume in the SCIAMACHY observations implies 414 the enhancement is in the upper troposphere where the NO_x 415 lifetime of a week is sufficient for long-range transport. The 416 feature persists if a more strict cloud filter is applied to the 417 SCIAMACHY NO₂ measurements. The GEOS-Chem simu- 418 lation with 0.4 Tg N yr⁻¹ from midlatitude lightning 419 shows little enhancement. Indeed, the underestimate in that 420 simulation with respect to in situ measurements of upper 421 tropospheric NO₂ was attributed to an underestimate in 422 lightning NO_x emissions in section 3.2. The simulation with 423 1.6 Tg N yr⁻¹ better simulates the NO₂ plume in the 424 SCIAMACHY observations, but does not capture its mag- 425 nitude nor spatial extent. The remaining bias likely arises 426 from insufficient altitude of lightning NO_x emissions which 427

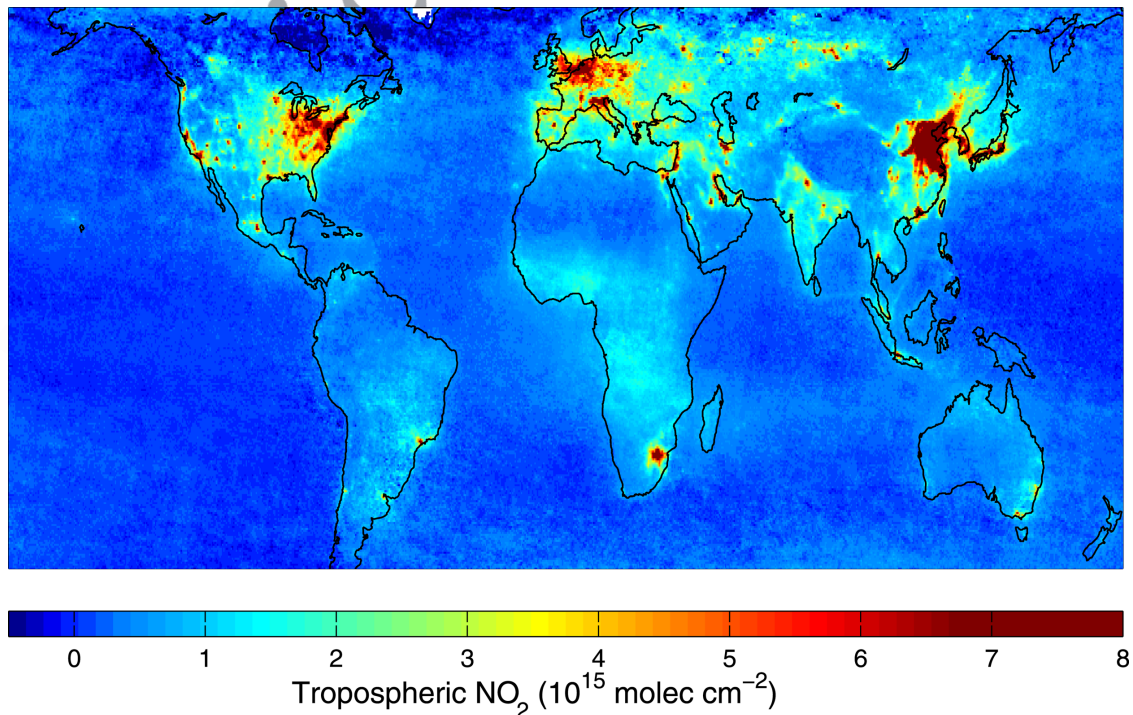


Figure 4. Mean tropospheric NO₂ columns retrieved from the SCIAMACHY satellite instrument for May 2004 to April 2005. Scenes where clouds or snow dominate solar backscatter have been excluded from the average to reduce retrieval uncertainty.

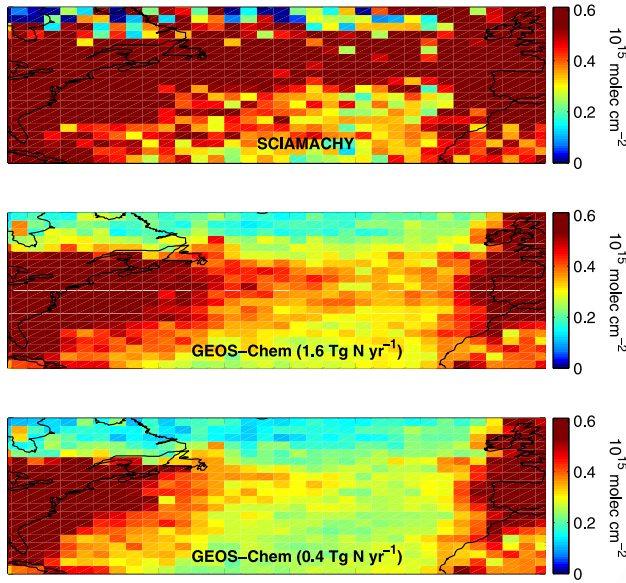


Figure 5. Tropospheric NO₂ columns over the North Atlantic Ocean averaged over May–October 2004 as (top) retrieved from SCIAMACHY, (middle) calculated with the GEOS-Chem model using 1.6 Tg N yr⁻¹ from lightning at northern midlatitudes, and (bottom) calculated with the GEOS-Chem model using 0.4 Tg N yr⁻¹ from lightning at northern midlatitudes. Scenes where clouds or snow dominate SCIAMACHY observations of solar backscatter have been excluded from the average to reduce retrieval uncertainty.

would decrease the NO_x lifetime and the spatial extent of the plume, consistent with our interpretation from comparison with the DC-8 measurements. Hudman et al. (manuscript in preparation, 2006) further investigate this issue in the GEOS-Chem simulation.

4. A Posteriori NO_x Emission Inventory

4.1. Approach to Produce the A Posteriori Inventory

[23] Following *Martin et al.* [2003b], we determine the local top-down surface NO_x emissions E_t for May 2004 to April 2005 from the local retrieved NO₂ columns Ω_r through the following linear relationship:

$$E_t = \alpha \Omega_r, \quad (1)$$

where the coefficient $\alpha = (\Omega_{\text{NO}_x}/\Omega_{\text{NO}_2})/\tau_{\text{NO}_x}$ is determined with the GEOS-Chem chemical mechanism by sampling the model at the SCIAMACHY observation time using the simulation with a priori emissions $\alpha = E_a/\Omega_a$. This simple approach yields an effective NO_x lifetime τ_{NO_x} that accounts for local NO_x chemistry, NO_x transport, and a $\Omega_{\text{NO}_x}/\Omega_{\text{NO}_2}$ ratio that accounts for free tropospheric NO_x sources as represented by the GEOS-Chem model. This approach takes advantage of the short NO_x lifetime in the lower mixed layer of less than a day that is inferred from in situ measurements [*Ryerson et al.*, 2003] and expected from model calculations during most of the year [*Martin et al.*, 2003b]. For a horizontal wind speed of 10 m/s, the corresponding smearing length scale [*Palmer et al.*, 2003]

ranges from 50 km in summer to 250 km in winter, comparable to the scale of the model grid. The SCIAMACHY data are regridded to the GEOS-Chem resolution before application of equation (1). We apply equation (1) only over land and coastal regions. Inference of oceanic surface NO_x emissions would be prone to excessive error due to the large relative contribution of lightning to the NO₂ column over ocean as apparent in Figures 2 and 5.

[24] A possible concern is the degree of nonlinearity in the relationship between the rate of surface NO_x emissions and the NO₂ column over a range of NO_x emissions. NO_x concentrations respond nonlinearly to changes in emissions due to feedbacks on OH [*Kunhikrishnan and Lawrence*, 2004]. However, NO₂ would be expected to respond more linearly than NO_x to changes in emissions owing to compensation in the NO₂/NO_x ratio that results from feedbacks on hydroxyl radicals and O₃. We quantify the combination of these two effects with the GEOS-Chem model.

[25] Figure 6 shows the simulated NO₂ column as a function of the NO_x emission rate for December and July at six different locations. The slope of the line indicates the local value of α in equation (1). The greater slope in winter is due to the longer NO_x lifetime. Biomass burning emissions in January contribute to the large seasonal variation in Nigeria. The exact calculations indicated by circles and stars show highly linear relationships that are consistent to within 10% of the local relationship used in equation (1). A simulation at higher spatial resolution should better account for spatial variation in the relationship between NO₂ columns and NO_x emissions, and may yield a more nonlinear relationship over urban areas.

[26] Table 3 provides regional and global totals in the top-down inventory. Global top-down NO_x emissions are 46% higher than the a priori. The largest regional increase (6.0 Tg N yr⁻¹) is found in East Asia. We further investigate these differences in the next section.

[27] The a posteriori inventory E is calculated from the top-down and bottom-up inventories, weighting by their relative uncertainty. Assuming a lognormal distribution of errors in the a priori ε_a and top-down ε_t yields

$$\ln E = \frac{(\ln E_t)(\ln \varepsilon_a)^2 + (\ln E_a)(\ln \varepsilon_t)^2}{(\ln \varepsilon_a)^2 + (\ln \varepsilon_t)^2}, \quad (2)$$

with a corresponding relative error ε

$$(\ln \varepsilon)^{-2} = (\ln \varepsilon_a)^{-2} + (\ln \varepsilon_t)^{-2}. \quad (3)$$

[28] We calculate the total uncertainty in the top-down emission inventory by adding in quadrature the uncertainty in the NO₂ retrieval, in the calculation of α , and in the representativeness of α . Section 3.1 described the uncertainty in the NO₂ retrieval of $\pm(5 \times 10^{14})$ molecules cm⁻² + 30%. Previous comparison of the GEOS-Chem simulations of the NO_x/NO_y ratio over and downwind of North America [*Fiore et al.*, 2002; *Li et al.*, 2004; Hudman et al., manuscript in preparation, 2006] and East Asia [*Wang et al.*, 2004] suggests that the uncertainty in the calculation of α is 30%. We add in quadrature an additional 10% error for the representativeness of α based on the comparison in Figure 6.

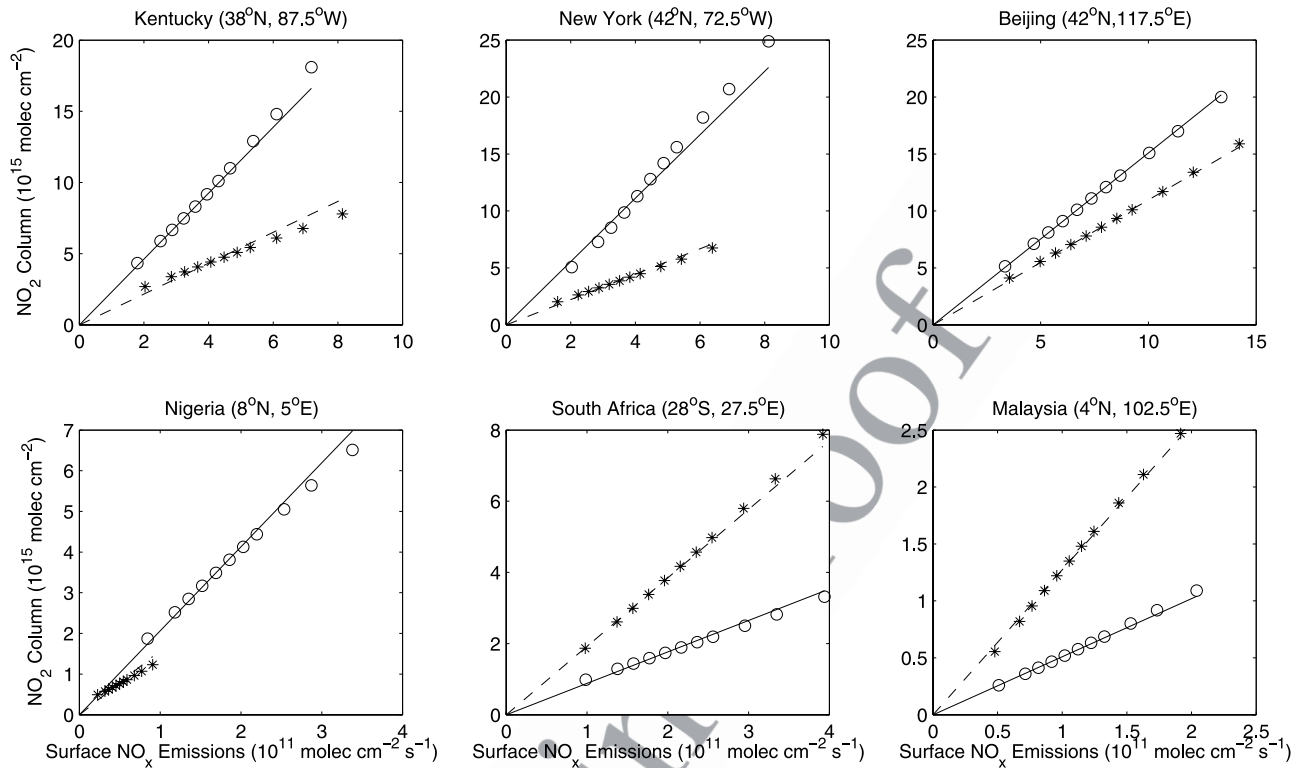


Figure 6. Local relationship between modeled NO₂ columns and NO_x emissions at six different locations at 1000 local time during January (solid lines and circles) and July (dashed lines and stars). Lines show the linear relationship used in equation (1) to infer top-down NO_x emissions from retrieved NO₂ columns. Circles and stars show the NO₂ column calculated with sensitivity simulations in which surface NO_x emissions were varied within a factor of 2 of the standard simulation.

512 The total uncertainty in the top-down inventory is less than
 513 50% over regions with enhanced NO₂ and increases to more
 514 than a factor of 2 over remote regions.

515 [29] The uncertainty in the a priori inventory is not
 516 available. The uncertainty in biomass burning and soil
 517 NO_x emissions is taken to be a factor of 3, reflecting the
 518 range of global estimates [Prather *et al.*, 2001]. We estimate
 519 the local uncertainty in the fossil fuel inventory based on
 520 comparison with the recently available EDGAR 3.2FT2000

inventory [Olivier, 2005]; values are about 50% over major 521
 industrial areas and higher elsewhere similar to Martin *et al.* 522
 [2003b]. An additional 10% error is applied here to reflect 523
 the outdated a priori; our resultant a posteriori inventory 524
 increases by 0.2 Tg N yr⁻¹ as a result of the decreased 525
 weighting of the bottom-up inventory compared with the 526
 top-down inventory. Similarly, an additional 30% error is 527
 applied here to Chinese emissions in light of potentially 528
 unrepresented sources inferred from aircraft and surface 529

t3.1 **Table 3.** Annual Mean Regional NO_x Emissions (and Relative Errors)^a

t3.2	A Priori	SCIAMACHY	A Posteriori	EDGAR ^b	M2003 ^c	J2005 ^d
t3.3 East Asia	6.7 (2.8)	12.7 (1.6)	9.8 (1.7)	8.2	7.3	7.6
t3.4 North America	8.0 (1.9)	9.7 (1.6)	8.7 (1.5)	7.3	8.4	8.5
t3.5 Europe	6.4 (2.1)	10.2 (1.5)	8.2 (1.5)	9.2	7.2	7.0
t3.6 Africa	6.9 (2.5)	9.2 (1.8)	8.1 (1.7)	7.8	7.4	8.5
t3.7 SE Asia and India	4.8 (2.3)	5.5 (1.9)	4.7 (1.7)	4.6	3.4	3.6
t3.8 South America	4.0 (2.5)	5.3 (2.1)	4.7 (1.8)	4.9	3.2	3.7
t3.9 Australia	1.1 (2.7)	2.8 (2.0)	1.9 (1.8)	1.2	1.0	1.2
t3.10 Total	37.9 (2.3)	55.4 (1.8)	46.1 (1.6)	43.2	37.7	40.1

^aUnits are Tg N yr⁻¹. Relative errors represent the geometric standard deviation about the mean. Region boundaries follow standard convention. Emissions include all land surface sources (fossil fuel combustion, biofuels, biomass burning, and soils) and exclude nonsurface sources (lightning, aircraft, and stratosphere).

t3.11 ^bThe EDGAR 3.2FT2000 inventory only includes fossil fuel, biomass burning, and biofuel emissions. We add the GEOS-Chem soil NO_x emissions here for consistency.

t3.13 ^cA posteriori emission inventory is from Martin *et al.* [2003b] based on GOME 1996–1997 NO₂ columns.

t3.14 ^dA posteriori emission inventory is from Jaeglé *et al.* [2005] based on GOME 2000 NO₂ columns.

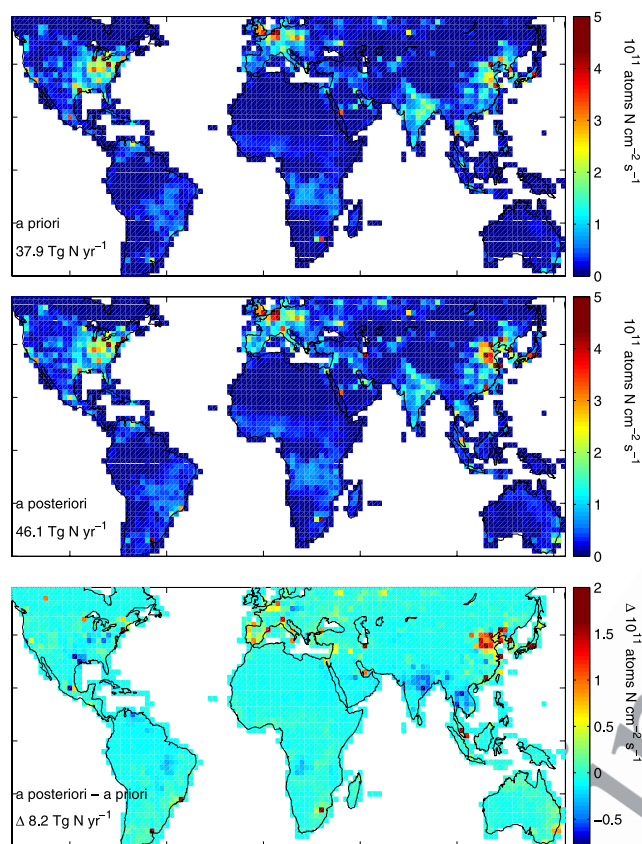


Figure 7. Average NO_x emissions at $2^\circ \times 2.5^\circ$ horizontal resolution for the (top) a priori and (middle) a posteriori inventories. Only surface NO_x emissions are included; nonsurface emissions from lightning, aircraft, and the stratosphere are excluded. Annual global emissions are indicated in the bottom left. (bottom) Difference between the a posteriori and a priori inventories.

530 measurements by Wang *et al.* [2004]; our resultant a
531 posteriori inventory increases by 0.4 Tg N yr^{-1} .

532 [30] Table 3 provides regional and global uncertainties.
533 The global relative uncertainty in the top-down inventory is
534 a factor of 2.3, compared with a factor of 1.8 in the a priori,
535 resulting in more influence from SCIAMACHY than the
536 bottom-up inventory in the calculation of the a posteriori.

537 4.2. Discussion of the A Posteriori Inventory

538 [31] Figure 7 shows the a priori and a posteriori invento-
539 ries of land surface emissions. Land surface emissions here
540 include contributions from fossil fuels, biofuels, biomass
541 burning, and soils; they exclude contributions from light-
542 ning, aircraft, or the stratosphere. The global total of the a
543 posteriori ($46.1 \text{ Tg N yr}^{-1}$) is 22% higher than the a priori.
544 The two inventories exhibit a high degree of consistency
545 ($r^2 = 0.81$). We find little evidence of horizontal smearing in
546 the a posteriori inventory which should be most apparent at
547 high latitudes along prevailing wind directions.

548 [32] Table 3 provides regional totals. A posteriori emis-
549 sions from East Asia exceed those from either North
550 America or Europe. Soils and biomass burning explain
551 most of Africa's relatively large surface emissions [Jaeglé

et al., 2005]. The estimate of the global uncertainty in NO_x 552
emissions is reduced from a factor of 2.3 in the a priori to a 553
factor of 1.6 in the a posteriori as calculated with 554
equation (3). 555

[33] The bottom panel of Figure 7 shows the difference 556
between the a priori and a posteriori inventories. Most 557
regions of the world exhibit little change. However, pro- 558
nounced differences in NO_x emissions are apparent over 559
numerous major industrial areas including Beijing, Tokyo, 560
Buenos Aires, and New York City. The a posteriori is a 561
factor of 2 larger than the a priori for Shanghai, Hong Kong, 562
Tehran, and Sao Paulo. Discrepancies were noted in many 563
of these regions in a previous comparison of the a priori 564
with GOME [Martin *et al.*, 2003b], although less clearly 565
owing to its coarse spatial resolution. Regions with annual 566
mean emissions of more than 2×10^{11} molecules $\text{cm}^{-2} \text{ s}^{-1}$ 567
account for 40% of the difference between the a priori and a 568
posteriori inventories. The comparison of NO₂ columns 569
determined from SCIAMACHY and in situ measurements 570
in Figure 3 suggests that NO_x emissions could be even 571
higher over megacities. The biases found here reflect a 572
combination of imperfect information in the GEIA inven- 573
tory, and recent changes in emissions unaccounted for in the 574
a priori. Rapid growth of the Asian transportation sector is 575
leading to a rapid rise in NO_x emissions [Akimoto, 2003; 576
Streets *et al.*, 2003]. Oil consumption by the Chinese road 577
transport system increased at an average annual growth rate 578
of 9% over 1997–2002 [He *et al.*, 2005]. Richter *et al.* 579
[2005] examined trends in tropospheric NO₂ columns from 580
GOME and found an increase of 50% over industrial China 581
during 1996–2002, with an accelerating increase in latter 582
years. In contrast, a posteriori emissions from the Ohio 583
River Valley of the United States are 10–25% lower than 584
the a priori as expected from controls on NO_x emissions 585
from electric utilities [Environmental Protection Agency, 586
2003] and by trends in GOME NO₂ columns [Richter *et al.*, 587
et al., 2005]. Modest decreases in the a posteriori with respect 588
to the a priori are found over biomass burning regions of 589
South America, Central Africa, and South Asia, consistent 590
with previous inversions [Martin *et al.*, 2003b; Jaeglé *et al.*, 591
2005; Müller and Stavrou, 2005]. 592

[34] Figure 8 shows the seasonal variation in the a 593
posteriori inventory. A posteriori NO_x emissions in the 594
southern tropics are most intense during May–October, 595
and in the northern tropics during November–April, as 596
expected from satellite observations of fires [Duncan *et al.* 597

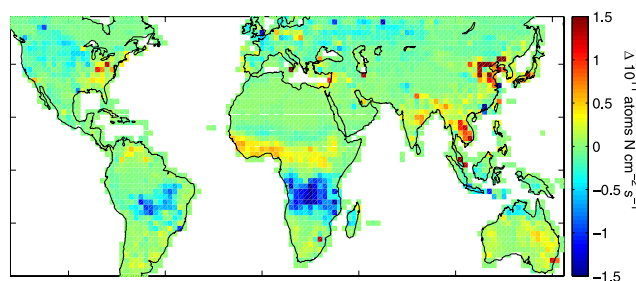


Figure 8. Seasonal change in a posteriori NO_x emissions as determined for November 2004 to April 2005 minus May–October 2004.

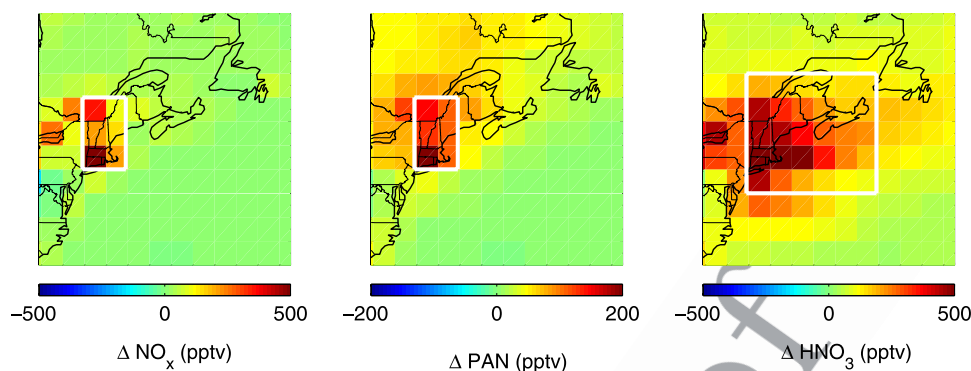


Figure 9. Difference in the GEOS-Chem model simulation of NO_x, PAN, and HNO₃ over the period 5 July 2004 to 15 August 2004 in the lower troposphere (~600 m) using the a posteriori inventory minus the simulation using the a priori inventory. White boxes indicate the regions over which model and aircraft are compared in Figure 10.

598 *al.*, 2003]. Industrial regions are of particular interest here. 600
 599 The fossil fuel inventory is aseasonal in the a priori, 600
 however wintertime NO_x emissions in the a posteriori are 601
 larger than in the a priori by 50% near Beijing, and by 20– 602
 30% in the eastern United States. *Jaeglé et al.* [2005] and 603
Richter et al. [2005] also found evidence of a wintertime 604
 maximum in Chinese NO_x emissions. Reductions in NO_x 605
 emissions from power plants are expected during May– 606
 September in the eastern United States with the largest 607
 changes along the Ohio River Valley [*Environmental Pro-* 608
tection Agency, 2003; *Frost et al.*, 2006].

609 [35] We reassess the effect of nonlinearity in equation 610
 (1) by incorporating the a posteriori inventory into the 611
 GEOS-Chem model, conducting a new simulation, and 612
 reapplying equations (1)–(3). The resultant top-down 613
 inventory increases by less than 5%, as expected from 614
 Figure 6. Small decreases in the resultant top-down 615
 inventory over major industrial areas are compensated by 616
 small increases elsewhere. As previously noted, a more 617
 nonlinear relationship may be expected in a higher res- 618
 olution simulation.

619 [36] Sharp spatial gradients in NO_x chemistry also could 620
 affect the inference of emissions from SCIAMACHY NO₂ 621
 columns. We examine the potential sensitivity to model 622
 resolution by shifting the model grid by half of a grid box 623
 and repeating the analysis. The resultant a posteriori inven- 624
 tory decreases by 2%. Increases in NO_x emissions from 625
 some cities such as Los Angeles are compensated by 626
 decreases from others such as New York City.

627 [37] A recently submitted manuscript [*van Noije et al.*, 628
 2006] reveals that tropospheric NO₂ columns retrieved from 629
 GOME by the Dalhousie/SAO, BIRA/KNMI, and Bremen 630
 groups are generally consistent during summer but exhibit 631
 large systematic differences over industrial regions during 632
 wintertime. NO₂ columns retrieved by Dalhousie/SAO over 633
 industrial regions during wintertime tend to be systemati- 634
 cally lower by 50% to 100% than those retrieved from either 635
 the other groups. If those systematic biases exist between 636
 the different SCIAMACHY retrievals, NO_x emissions inferred 637
 from NO₂ columns retrieved by the BIRA/KNMI and 638
 Bremen groups over industrial regions during winter would 639
 be correspondingly larger than inferred here. Additional

validation and intercomparison of SCIAMACHY retrievals 640
 is needed. 641

4.3. Evaluation of the A Posteriori Inventory 642

[38] We evaluate the a posteriori inventory by comparison 643
 with airborne in situ measurements, using the GEOS-Chem 644
 model as an intermediary. We focus on the region near New 645
 York City where the a priori and a posteriori inventories 646
 exhibited large differences and airborne measurements are 647
 available as part of ICARTT. Chemical ionization mass 648
 spectrometers on the WP-3D aircraft were used to measure 649
 PAN [*Flocke et al.*, 2005] and gas-phase HNO₃ [*Neuman et* 650
al., 2002]. 651

[39] We include into the GEOS-Chem model the a 652
 posteriori inventory determined over May–October 2004, 653
 conduct a forward simulation, and examine the change in 654
 the simulation of reactive nitrogen. Figure 9 shows the 655
 resultant regional change in the GEOS-Chem simulation of 656
 NO_x, PAN, and HNO₃. The left panel shows that the largest 657
 change in NO_x occurs over the New York and Connecticut 658
 region where the largest change in emissions occurred. The 659
 middle panel shows a slightly more homogeneous increase 660
 in PAN of 100–200 pptv over most of New England. The 661
 right panel shows a more spatially uniform change in 662
 HNO₃, reflecting the longer HNO₃ lifetime of a few days 663
 in the lower troposphere. The simulated HNO₃ mixing ratio 664
 using the a posteriori inventory is 300–500 pptv larger over 665
 New England, Atlantic Canada, and into the North Atlantic 666
 Ocean. 667

[40] Figure 10 compares both the a priori and a posteriori 668
 inventories with in situ measurements taken as part of 669
 ICARTT. Both model and observations are averaged over 670
 the domains in which the a posteriori resulted in maximum 671
 differences in the model simulation as indicated by the 672
 white lines in Figure 9. In all three cases, the in situ 673
 measurements are more consistent with the a posteriori 674
 inventory than with the a priori. The mean model biases 675
 in the lower troposphere of NO_x and HNO₃ were reduced 676
 by 500 pptv, and by 200 pptv for PAN. 677

[41] We also evaluated the a posteriori inventory with in 678
 situ measurements from the DC-8 aircraft. Particular atten- 679
 tion was given to the Ohio River Valley and New England. 680

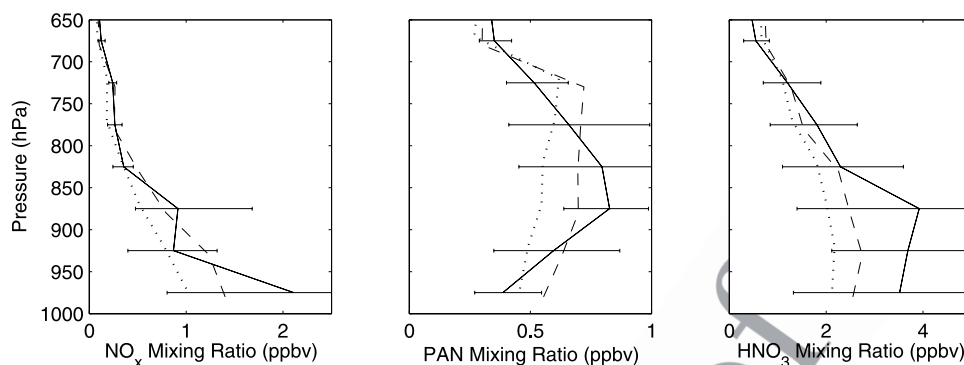


Figure 10. Mean vertical profiles of NO_x, PAN, and HNO₃ for the ensemble of WP-3D flights within the regions identified in Figure 9 over the period 5 July 2004 to 15 August 2004. Observations (solid lines, with 17th and 83rd percentiles as horizontal bars) are compared to model results sampled along the flight tracks at the measurement time using either the a priori NO_x inventory (dash-dotted lines) or the a posteriori NO_x inventory (dashed lines).

681 The comparison was inconclusive in all cases. Simulations
 682 of reactive nitrogen using either the a priori and a posteriori
 683 inventories exhibited little difference at the locations and
 684 times sampled by the DC-8 aircraft. Additional evaluation
 685 of the a posteriori inventory would be useful, especially
 686 downwind of China where pronounced differences exist
 687 versus the a priori.

689 5. Comparison of the A Posteriori With Previous 690 Inventories

691 [42] We compare the a posteriori inventory with three
 692 commonly used bottom-up emission inventories and with
 693 previous inversions from GOME NO₂ columns. Figure 11
 694 compares the a posteriori inventory with the EDGAR
 695 3.2FT2000 inventory for 2000 [Olivier *et al.*, 2005]. The
 696 two inventories are moderately consistent ($r^2 = 0.55$, $n =$
 697 3402). Part of the scatter arises from slight differences in the
 698 location of emissions in the two inventories in major
 699 industrial areas such as east China, northern Europe, and
 700 Houston. The global NO_x emission rate for the a posteriori
 701 inventory is 7% higher than that for EDGAR. A posteriori
 702 NO_x emissions tend to be higher than EDGAR emissions
 703 over industrial regions of the eastern United States, East
 704 Asia, and South Africa as well as numerous urban areas, but
 705 lower over Europe. The positive bias over the eastern
 706 United States in part reflects the influence of the outdated
 707 a priori on the a posteriori. Table 3 shows that regional
 708 totals in the a posteriori are generally more consistent with
 709 EDGAR than the a priori, likely reflecting more current
 710 information in EDGAR.

711 [43] Figure 12 compares the a posteriori inventory with
 712 the National Inventory for 1999 (NEI99) of the United
 713 States Environmental Protection Agency. The two inven-
 714 tories exhibit a high degree of consistency ($r^2 = 0.82$, $n =$
 715 192). The a posteriori NO_x emission rate for the United
 716 States of 6.8 Tg N yr⁻¹ is 0.2 Tg N yr⁻¹ larger than that of
 717 NEI99. A posteriori NO_x emissions are about 25% lower
 718 than those for NEI99 over most of the eastern United States
 719 as expected from reductions in power plant emissions not
 720 included in NEI99 [Environmental Protection Agency,
 721 2003; Frost *et al.*, 2006]. These decreases are compensated
 722 by higher NO_x emissions in the a posteriori than NEI99 for

urban areas as may be associated with a hypothesized 723
 underestimate in mobile emissions [Parrish *et al.*, 2002], 724
 and for agricultural areas supporting earlier evidence of an 725
 underestimate in soil NO_x emissions [Martin *et al.*, 2003b; 726
 Jaeglé *et al.*, 2005]. 727

[44] Figure 13 compares the a posteriori inventory with 728
 the bottom-up inventory of Streets *et al.* [2003] for eastern 729
 Asia for the year 2000. The spatial distribution of the two 730
 inventories is moderately consistent ($r^2 = 0.64$, $n = 660$). 731
 However, the regional magnitude of the a posteriori inven- 732
 tory of 14.3 Tg N yr⁻¹ is 68% larger than that of Streets *et* 733
al. [2003]. Wang *et al.* [2004] previously applied measure- 734
 ments of reactive nitrogen from the Transport and Chemical 735
 Evolution over the Pacific (TRACE-P) aircraft mission over 736

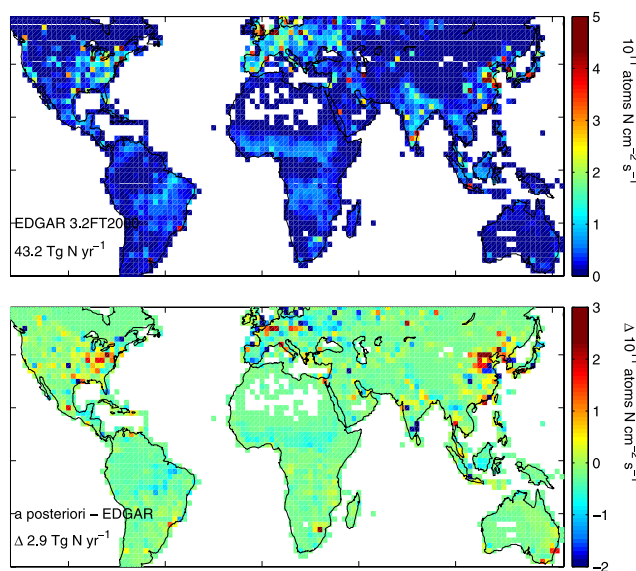


Figure 11. (top) Average surface NO_x emissions at 2° × 2.5° horizontal resolution from the EDGAR 3.2FT2000 inventory. The EDGAR inventory only includes industrial, biomass burning, and biofuel emissions. We add the GEOS-Chem soil NO_x emissions here for consistency. Annual global emissions are indicated in the bottom left. (bottom) Difference between the a posteriori and a priori inventories.

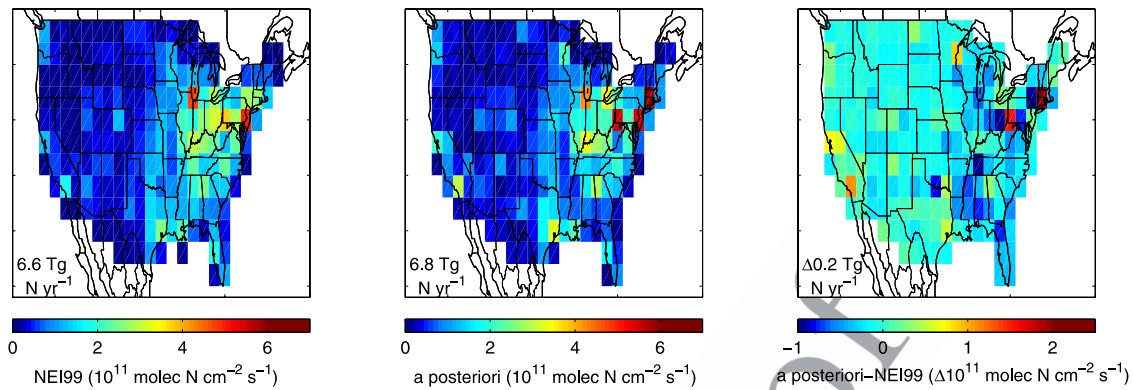


Figure 12. Annual average surface NO_x emissions at $2^\circ \times 2.5^\circ$ horizontal resolution for the United States (left) from the National Emission Inventory for 1999 (NEI99) and (middle) from the a posteriori inventory. Annual regional totals are indicated in the bottom left. (right) Difference between the two inventories.

737 the northwest Pacific and from two ground stations during
 738 spring 2001 to constrain Asian NO_x emissions and found
 739 evidence for a 47% increase in Chinese NO_x emissions with
 740 respect to *Streets et al.* [2003]. The larger difference found
 741 here likely reflects recent growth in Asian NO_x emissions.
 742 [45] Table 3 shows the regional totals in two a posteriori
 743 inventories determined from GOME NO₂ columns for
 744 1996–1997 by *Martin et al.* [2003b], and for 2000 by
 745 *Jaeglé et al.* [2005]. The a posteriori inventory determined
 746 from SCIAMACHY is higher than that determined from
 747 GOME for most regions, likely reflecting recent global
 748 growth in NO_x emissions. Differences in the two measure-
 749 ments could also play a role in the higher SCIAMACHY
 750 inventory.

751 6. Conclusions

752 [46] We have constructed an improved inventory of
 753 current surface land NO_x emissions by combining top-down
 754 information from the SCIAMACHY satellite instrument
 755 with a priori information from a bottom-up inventory.
 756 Tropospheric NO₂ columns were retrieved from

SCIAMACHY to provide the top-down constraint. The
 top-down constraint was determined over May 2004 to
 April 2005 to include the ICARTT campaign. Top-down
 emissions were determined through a simple inversion with
 a global chemical transport model (GEOS-Chem).
 [47] We validated the tropospheric NO₂ columns with
 coincident in situ measurements from the NASA DC-8 and
 the NOAA WP-3D aircraft as part of the ICARTT cam-
 paign. Nearly 20 coincident measurements were found,
 providing an unprecedented validation opportunity over a
 wide range of conditions ranging from remote marine to
 highly polluted. The two measurements techniques were
 consistent within their uncertainty ($r^2 = 0.60$, geometric
 mean = 0.82, slope = 0.82). The SCIAMACHY columns
 tended to be lower than those determined from in situ
 measurements over polluted regions, and higher over re-
 mote regions, suggesting that NO_x emissions from mega-
 cities may be higher than reported here. As part of the
 validation, GEOS-Chem simulated vertical profiles of NO₂
 used in the retrieval air mass factor calculation were
 compared with in situ measurements. A northern midlati-
 tude lightning source of 1.6 Tg N yr⁻¹ reduced the

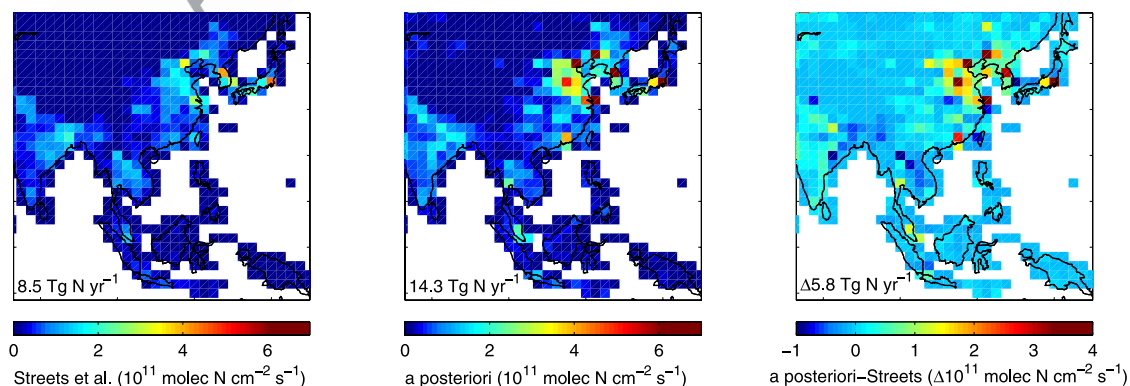


Figure 13. Annual average surface NO_x emissions at $2^\circ \times 2.5^\circ$ horizontal resolution for eastern Asia from (left) the *Streets et al.* [2003] and (middle) the a posteriori inventory. The *Streets et al.* [2003] inventory only includes industrial and biofuel emissions. We add the GEOS-Chem soil and biomass burning NO_x emissions here for consistency. Annual regional totals are indicated in the bottom left. (right) Difference between the two inventories.

779 difference between airborne and simulated profiles; remain-
780 ing differences would affect the retrieved NO₂ columns by a
781 few percent.

782 [48] The increase in the simulated NO₂ columns from
783 increased lightning NO_x emissions also reduced a model
784 bias versus SCIAMACHY NO₂ columns over the North
785 Atlantic Ocean where lightning makes a large relative
786 contribution to the NO₂ column. SCIAMACHY NO₂ col-
787 umns show a weak plume from North American lightning
788 NO_x emissions that extends across the North Atlantic Ocean
789 to Europe.

790 [49] Tropospheric NO₂ columns are highly heterogeneous
791 over regions with isolated surface sources, providing em-
792 pirical evidence of the short NO_x lifetime and high NO₂/
793 NO_x ratio in the lower mixed layer that facilitate mapping of
794 NO_x emissions from observed NO₂ columns over land. We
795 evaluated the local relationship between NO₂ columns and
796 land surface NO_x emissions by conducting sensitivity sim-
797 ulations over a range of emissions. We found a highly linear
798 relationship at the resolution of 2° × 2.5° used here; errors
799 in the top-down estimate due to nonlinearity in the rela-
800 tionship about the a priori are less than 10% for a variety of
801 locations.

802 [50] Our a posteriori inventory of 46.1 Tg N yr⁻¹ is 22%
803 higher than the GEIA-based a priori for 1998. Much of the
804 increase is driven by emissions from East Asia. A posteriori
805 NO_x emissions from East Asia (9.8 Tg N yr⁻¹) exceed those
806 from North America or Europe. Comparison of the a
807 posteriori and a priori inventory reveals significant under-
808 estimates in the a priori over several megacities outside of
809 East Asia. The estimate of the global uncertainty in NO_x
810 emissions is reduced from a factor of 2.3 in the a priori to a
811 factor of 1.6 in the a posteriori.

812 [51] We evaluated the a posteriori inventory by including
813 it in the GEOS-Chem model and comparing the resultant
814 simulation over and downwind of New York City with in
815 situ airborne measurements. The a posteriori inventory
816 reduced the regional model bias in the lower troposphere
817 of NO_x by 500 pptv, of PAN by 200 pptv, and of HNO₃ by
818 500 pptv, providing regional confidence in the a posteriori.

819 [52] We compared the a posteriori inventory with three
820 other bottom-up inventories. The a posteriori inventory is
821 7% higher than that of the global EDGAR 3.2FT2000 for
822 the year 2000, with pronounced differences over major
823 industrial and urban areas. The a posteriori inventory of
824 6.8 Tg N yr⁻¹ for the United States is 3% higher than the
825 National Emission Inventory for 1999 of the Environmental
826 Protection Agency. Higher NO_x emission rates in the urban
827 centers and agricultural areas are offset by lower regional
828 NO_x emission rates from much of the eastern United States.
829 The a posteriori inventory for eastern Asia is 68% larger
830 than that of *Streets et al.* [2003] for 2001 with most of the
831 difference arising from major urban and industrial centers.

832 [53] Limitations in the current work that could introduce
833 systematic errors in the a posteriori include possible biases
834 in the cloud retrieval and surface reflectivity data set, zonal
835 variability in the stratospheric NO₂ column, the outdated a
836 priori, coarse model resolution, and horizontal smearing of
837 the relationship between NO₂ columns and NO_x emissions.
838 The development of a cloud retrieval that treats clouds as a
839 collection of Mie scatterers rather than Lambertian surface
840 would enable a more accurate air mass factor calculation. A

higher resolution surface reflectivity data set would better 841
resolve spatial heterogeneity in urban areas. Representation 842
of zonal variability in the stratospheric NO₂ column should 843
improve the a posteriori inventory at high latitudes during 844
winter. A more current a priori that accounts for recent 845
trends in NO_x emissions would yield a more accurate a 846
posteriori. Simulations at higher spatial resolution would 847
better resolve the large spatial heterogeneity of urban areas 848
apparent from SCIAMACHY observations, and better ac- 849
count for spatial variation in the NO_x lifetime in the 850
inversion. An inverse analysis that quantitatively accounts 851
for horizontal smearing should improve the accuracy of the 852
inversion. Observations at higher resolution of 13 km by 24 853
km from the Ozone Monitoring Instrument onboard the 854
Aura satellite soon will provide even greater detail and 855
improve cloud screening. 856

[54] **Acknowledgments.** Three anonymous reviewers and Mark Law- 857
rence provided constructive comments that improved the manuscript. We 858
are grateful to the TEMIS project for making the FRESKO cloud fields 859
publicly available. We thank the Netherlands SCIAMACHY Data Center 860
(NL-SCIA-DC) for providing data and processing services. This work was 861
supported by NASA's Radiation Science Program. The GEOS-Chem model 862
is managed by the Atmospheric Chemistry Modeling Group at Harvard 863
University with support from the NASA Atmospheric Chemistry Modeling 864
and Analysis Program. 865

References

- Adams, P. J., J. H. Seinfeld, D. Koch, L. Mickley, and D. Jacob (2001), 867
General circulation model assessment of direct radiative forcing by the 868
sulfate-nitrate-ammonium-water inorganic aerosol system, *J. Geophys.* 869
Res., *106*, 1097–1112. 870
- Akimoto, H. (2003), Global air quality and pollution, *Science*, *302*, 1716– 871
1719. 872
- Alexander, B., J. Savarino, C. C. W. Lee, R. J. Park, D. J. Jacob, M. H. 873
Thiemens, Q. B. Li, and R. M. Yantosca (2005), Sulfate formation in sea- 874
salt aerosols: Constraints from oxygen isotopes, *J. Geophys. Res.*, *110*, 875
D10307, doi:10.1029/2004JD005659. 876
- Beirle, S., U. Platt, M. Wenig, and T. Wagner (2003), Weekly cycle of NO₂ 877
by GOME measurements: A signature of anthropogenic sources, *Atmos.* 878
Chem. Phys., *3*, 2225–2232. 879
- Beirle, S., U. Platt, M. Wenig, and T. Wagner (2004a), NO_x production by 880
lightning estimated with GOME, *Adv. Space Res.*, *34*(4), 793–797. 881
- Beirle, S., U. Platt, R. von Glasow, M. Wenig, and T. Wagner (2004b), 882
Estimate of nitrogen oxide emissions from shipping by satellite remote 883
sensing, *Geophys. Res. Lett.*, *31*, L18102, doi:10.1029/2004GL020312. 884
- Beirle, S., et al. (2005), Estimating the NO_x produced by lightning from 885
GOME and NLDN data: A case study in the Gulf of Mexico, *Am. Chem.* 886
Phys. Discuss., *5*, 11,295–11,329. 887
- Benkovitz, C. M., M. T. Scholtz, J. Pacyna, L. Tarrason, J. Dignon, E. C. 888
Voldner, P. A. Spiro, J. A. Logan, and T. E. Graedel (1996), Global 889
gridded inventories for anthropogenic emissions of sulfur and nitrogen, 890
J. Geophys. Res., *101*, 29,239–29,253. 891
- Berntsen, T. K., I. S. A. Isaksen, G. Myhre, S. Fuglestvedt, F. Stordal, 892
T. Alsвик Larson, R. S. Freckleton, and K. P. Shine (1997), Effects of 893
anthropogenic emissions on tropospheric ozone and its radiative forcing, 894
J. Geophys. Res., *102*, 28,101–28,126. 895
- Bey, I., et al. (2001), Global modeling of tropospheric chemistry with 896
assimilated meteorology: Model description and evaluation, *J. Geophys.* 897
Res., *106*, 23,073–23,096. 898
- Boersma, K. F., H. J. Eskes, and E. J. Brinksma (2004), Error analysis for 899
tropospheric NO₂ retrieval from space, *J. Geophys. Res.*, *109*, D04311, 900
doi:10.1029/2003JD003962. 901
- Boersma, K. F., H. J. Eskes, E. W. Meijer, and H. Kelder (2005), Estimates 902
of lightning NO_x production from GOME satellite observations, *Am.* 903
Chem. Phys. Discuss., *5*, 3047–3104. 904
- Bogumil, K., et al. (2003), Measurements of molecular absorption spectra 905
with the SCIAMACHY pre-flight model: Instrument characterization and 906
reference data for atmospheric remote-sensing in the 230–2380 nm re- 907
gion, *J. Photochem. Photobiol. A*, *157*, 167–184. 908
- Bovensmann, H., J. P. Burrows, M. Buchwitz, J. Frerick, V. V. Rozanov, 909
K. V. Chance, and A. P. H. Goede (1999), SCIAMACHY: Mission 910
objectives and measurement modes, *J. Atmos. Sci.*, *56*, 127–150. 911

- 912 Brasseur, G. P., J. T. Kiehl, J.-F. Muller, T. Schneider, C. Granier, X. X. Tie,
913 and D. Hauglustaine (1998), Past and future changes in global tropo-
914 spheric ozone: Impact on radiative forcing, *Geophys. Res. Lett.*, *25*,
915 3807–3810.
- 916 Burrows, J. P., et al. (1999), The Global Ozone Monitoring Experiment
917 (GOME): Mission concept and first scientific results, *J. Atmos. Sci.*, *56*,
918 151–175.
- 919 Chance, K. (1998), Analysis of BrO measurements from the Global Ozone
920 Monitoring Experiment, *Geophys. Res. Lett.*, *25*, 3335–3338.
- 921 Chance, K. V., and R. J. D. Spurr (1997), Ring effect studies: Rayleigh
922 scattering, including molecular parameters for rotational Raman scatter-
923 ing, and the Fraunhofer spectrum, *Appl. Opt.*, *36*, 5224–5230.
- 924 Choi, Y., Y. Wang, T. Zeng, R. V. Martin, T. P. Kurosu, and K. Chance
925 (2005), Evidence of lightning NO_x and convective transport of pollutants
926 in satellite observations over North America, *Geophys. Res. Lett.*, *32*,
927 L02805, doi:10.1029/2004GL021436.
- 928 Christian, H. J., et al. (2003), Global frequency and distribution of lightning
929 as observed from space by the Optical Transient Detector, *J. Geophys.*
930 *Res.*, *108*(D1), 4005, doi:10.1029/2002JD002347.
- 931 DeCaria, A. J., K. E. Pickering, G. L. Stenchikov, and L. E. Ott (2005),
932 Lightning-generated NO_x and its impact on tropospheric ozone produc-
933 tion: A three-dimensional modeling study of a Stratosphere-Troposphere
934 Experiment: Radiation, Aerosols and Ozone (STERAO-A) thunderstorm,
935 *J. Geophys. Res.*, *110*, D14303, doi:10.1029/2004JD005556.
- 936 Derwent, R. G., D. S. Stevenson, W. J. Collins, and C. E. Johnson (2004),
937 Intercontinental transport and the origins of the ozone observed at surface
938 sites in Europe, *Atmos. Environ.*, *38*, 1891–1901.
- 939 Duncan, B. N., R. V. Martin, A. C. Staudt, R. M. Yevich, and J. A. Logan
940 (2003), Interannual and seasonal variability of biomass burning emissions
941 constrained by remote-sensed observations, *J. Geophys. Res.*, *108*(D2),
942 4100, doi:10.1029/2002JD002378.
- 943 Edwards, D. P., et al. (2003), Tropospheric ozone over the tropical Atlantic:
944 A satellite perspective, *J. Geophys. Res.*, *108*(D9), 4237, doi:10.1029/
945 2002JD002927.
- 946 Environmental Protection Agency (1989), The 1985 NAPAP emission in-
947 ventory (version 2): Development of the annual data and modeler's tapes,
948 *EPA-600/7-89-012a*, Research Triangle Park, N. C.
- 949 Environmental Protection Agency (2003), National air quality and emis-
950 sions trends report: 2003 special studies edition, report, 190 pp., Research
951 Triangle Park, N. C.
- 952 European Space Agency (1995), *The GOME Users Manual*, edited by
953 F. Bednarz, ESA Publ. Div., Eur. Space Res. and Tech. Cent., Noordwijk,
954 Netherlands.
- 955 Evans, M. J., and D. J. Jacob (2005), Impact of new laboratory studies of
956 N₂O₅ hydrolysis on global model budgets of tropospheric nitrogen oxi-
957 des, ozone, and OH, *Geophys. Res. Lett.*, *32*, L09813, doi:10.1029/
958 2005GL022469.
- 959 Fehr, T., H. Holler, and H. Huntrieser (2004), Model study on production
960 and transport of lightning-produced NO_x in a EULINOX supercell storm,
961 *J. Geophys. Res.*, *109*, D09102, doi:10.1029/2003JD003935.
- 962 Fiore, A. M., D. J. Jacob, I. Bey, R. M. Yantosca, B. D. Field, and J. G.
963 Wilkinson (2002), Background ozone over the United States in summer:
964 Origin and contribution to pollution episodes, *J. Geophys. Res.*,
965 *107*(D15), 4275, doi:10.1029/2001JD000982.
- 966 Flocke, F. M., A. Swanson, A. W. Weinheimer, J. M. Roberts,
967 R. Schmitt, and S. Shertz (2005), On the measurement of PANs by
968 gas chromatography and electron capture detection, *J. Atmos. Chem.*,
969 *52*, 19–43.
- 970 Frost, G. J., et al. (2006), Effects of changing power plant NO_x emissions
971 on ozone in the eastern United States: Proof of concept, *J. Geophys. Res.*,
972 *111*, D12306, doi:10.1029/2005JD006354.
- 973 Greenblatt, G. D., J. J. Orlando, J. B. Burkholder, and A. R. Ravishankara
974 (1990), Absorption measurements of oxygen between 330 and 1140 nm,
975 *J. Geophys. Res.*, *95*, 18,577–18,585.
- 976 He, K. B., H. Huo, Q. Zhang, D. Q. He, F. An, M. Wang, and M. P. Walsh
977 (2005), Oil consumption and CO₂ emissions in China's road transport:
978 Current status, future trends, and policy implications, *Energy Policy*, *33*,
979 1499–1507.
- 980 Heue, K.-P., et al. (2005), Validation of SCIAMACHY tropospheric NO₂-
981 columns with AMAXDOAS measurements, *Atmos. Chem. Phys.*, *5*,
982 1039–1051.
- 983 Hirsch, R. M., and E. J. Gilroy (1984), Methods of fitting a straight line to
984 data: Examples in water resources, *Water Resour. Bull.*, *20*, 705–711.
- 985 Holland, E. A., and J.-F. Lamarque (1997), Modeling bio-atmospheric cou-
986 pling of the nitrogen cycle through NO_x emissions and NO_y deposition,
987 *Nutr. Cycl. Agroecosyst.*, *48*, 7–24.
- 988 Intergovernmental Panel on Climate Change (2001), *Climate Change 2001:*
989 *The Scientific Basis*, 881 pp., Cambridge Univ. Press, New York.
- 990 Jacob, D. J. (2000), Heterogeneous chemistry and tropospheric ozone, *At-*
991 *mos. Environ.*, *34*, 2131–2159.
- Jacob, D. J., et al. (1993), Simulation of summertime ozone over North
992 America, *J. Geophys. Res.*, *98*, 14,797–14,816.
- Jacob, D. J., et al. (1996), Origin of ozone and NO_x in the tropical tropo-
994 sphere: A photochemical analysis of aircraft observations over the South
995 Atlantic basin, *J. Geophys. Res.*, *101*, 24,235–24,250.
- Jacob, D. J., J. A. Logan, and P. P. Murti (1999), Effect of rising Asian
997 emissions on surface ozone in the United States, *Geophys. Res. Lett.*, *26*,
998 2175–2178.
- Jaeglé, L., et al. (2004), Satellite mapping of rain-induced nitric oxide
1000 emissions from soils, *J. Geophys. Res.*, *109*, D21310, doi:10.1029/
1001 2004JD004787.
- Jaeglé, L., L. Steinberger, R. V. Martin, and K. Chance (2005), Global
1003 partitioning of NO_x sources using satellite observations: Relative roles
1004 of fossil fuel combustion, biomass burning and soil emissions, *Faraday*
1005 *Discuss.*, *130*, 407–423, doi:10.1039/b502128f.
- Kasibhatla, P. S., H. Levy, W. J. Moxim, and W. L. Chameides (1991), The
1007 relative importance of stratospheric photochemical production on tropo-
1008 spheric NO_y levels: A model study, *J. Geophys. Res.*, *96*, 18,631–
1009 18,646.
- Koелеmeijer, R. B. A., P. Stammes, J. W. Hovenier, and J. F. de Haan
1011 (2002), Global distributions of effective cloud fraction and cloud top
1012 pressure derived from oxygen A band spectra measured by the Global
1013 Ozone Monitoring Experiment: Comparison to ISCCP data, *J. Geophys.*
1014 *Res.*, *107*(D12), 4151, doi:10.1029/2001JD000840.
- Koелеmeijer, R. B. A., J. F. de Haan, and P. Stammes (2003), A database of
1016 spectral surface reflectivity of the Earth in the range 335–772 nm derived
1017 from 5.5 years of GOME observations, *J. Geophys. Res.*, *108*, 4070,
1018 doi:10.1029/2002JD002429.
- Kunhikrishnan, T., and M. G. Lawrence (2004), Sensitivity of NO_x over the
1020 Indian Ocean to emissions from the surrounding continents and nonlinear-
1021 ities in atmospheric chemistry responses, *Geophys. Res. Lett.*, *31*,
1022 L15109, doi:10.1029/2004GL020210.
- Lelieveld, J., et al. (2002), Global air pollution crossroads over the Medi-
1024 terranean, *Science*, *298*, 794–799.
- Leue, C., M. Wenig, T. Wagner, O. Klimm, U. Platt, and B. Jahne (2001),
1026 Quantitative analysis of NO_x emissions from GOME satellite image se-
1027 quences, *J. Geophys. Res.*, *106*, 5493–5505.
- Li, Q. B., D. J. Jacob, R. M. Yantosca, J. W. Munger, and D. D. Parrish
1029 (2004), Export of NO_y from the North American boundary layer: Recon-
1030 ciling aircraft observations and global model budgets, *J. Geophys. Res.*,
1031 *109*, D02313, doi:10.1029/2003JD004086.
- Martin, R. V., et al. (2002a), Interpretation of TOMS observations of
1033 tropical tropospheric ozone with a global model and in-situ observations,
1034 *J. Geophys. Res.*, *107*(D18), 4351, doi:10.1029/2001JD001480.
- Martin, R. V., et al. (2002b), An improved retrieval of tropospheric nitrogen
1036 dioxide from GOME, *J. Geophys. Res.*, *107*(D20), 4437, doi:10.1029/
1037 2001JD001027.
- Martin, R. V., D. J. Jacob, R. M. Yantosca, M. Chin, and P. Ginoux (2003a),
1039 Global and regional decreases in tropospheric oxidants from photochem-
1040 ical effects of aerosols, *J. Geophys. Res.*, *108*(D3), 4097, doi:10.1029/
1041 2002JD002622.
- Martin, R. V., D. J. Jacob, K. Chance, T. P. Kurosu, P. I. Palmer, and M. J.
1043 Evans (2003b), Global inventory of nitrogen oxide emissions constrained
1044 by space-based observations of NO₂ columns, *J. Geophys. Res.*,
1045 *108*(D17), 4537, doi:10.1029/2003JD003453.
- Martin, R. V., et al. (2004), Evaluation of GOME satellite measurements of
1047 tropospheric NO₂ and HCHO using regional data from aircraft campaigns
1048 in the southeastern United States, *J. Geophys. Res.*, *109*, D24307,
1049 doi:10.1029/2004JD004869.
- Michaels, A. F., D. Olson, J. L. Sarmiento, J. W. Ammerman, K. Fanning,
1051 R. Jahnke, A. H. Knap, F. Lipschultz, and J. M. Prospero (1996), Inputs,
1052 losses and transformations of nitrogen and phosphorus in the pelagic
1053 North Atlantic Ocean, *Biogeochemistry*, *35*, 181–226.
- Müller, J.-F., and T. Stavrou (2005), Inversion of CO and NO_x emissions
1055 using the adjoint of the IMAGES model, *Am. Chem. Phys.*, *5*, 1157–
1056 1186.
- Murphy, D., D. Fahey, M. Proffitt, S. Liu, C. Eubank, S. Kawa, and
1058 K. Kelly (1993), Reactive odd nitrogen and its correlation with ozone
1059 in the lower stratosphere and upper troposphere, *J. Geophys. Res.*, *98*,
1060 8751–8773.
- Nenes, A., R. J. Charlson, M. C. Facchini, M. Kulmala, A. Laaksonen, and
1062 J. H. Seinfeld (2002), Can chemical effects on cloud droplet number rival
1063 the first indirect effect?, *Geophys. Res. Lett.*, *29*(17), 1848, doi:10.1029/
1064 2002GL015295.
- Neuman, J. A., et al. (2002), Fast-response airborne in situ measurements of
1066 HNO₃ during the Texas 2000 Air Quality Study, *J. Geophys. Res.*,
1067 *107*(D20), 4436, doi:10.1029/2001JD001437.
- Olivier, J. G. J., J. A. Van Aardenne, F. Dentener, L. Ganzeveld, and J. A.
1069 H. W. Peters (2005), Recent trends in global greenhouse gas emissions:
1070 Regional trends and spatial distribution of key sources, in *Non-CO₂*
1071

- 1072 *Greenhouse Gases (NCGG-4)*, edited by A. V. Amstel, pp. 325–330, 1124
 1073 Millpress, Rotterdam, Netherlands. 1125
- 1074 Palmer, P. I., et al. (2001), Air mass factor formulation for spectroscopic 1126
 1075 measurements from satellites: Application to formaldehyde retrievals 1127
 1076 from the Global Ozone Monitoring Experiment, *J. Geophys. Res.*, *106*, 1128
 1077 14,539–14,550. 1129
- 1078 Palmer, P. I., D. J. Jacob, A. M. Fiore, R. V. Martin, K. Chance, and T. P. 1130
 1079 Kurosu (2003), Mapping isoprene emissions over North America using 1131
 1080 formaldehyde column observations from space, *J. Geophys. Res.*, 1132
 1081 *108*(D6), 4180, doi:10.1029/2002JD002153. 1133
- 1082 Park, R. J., D. J. Jacob, M. Chin, and R. V. Martin (2003), Sources of 1134
 1083 carbonaceous aerosols over the United States and implications for natural 1135
 1084 visibility conditions, *J. Geophys. Res.*, *108*(D12), 4355, doi:10.1029/ 1136
 1085 2002JD003190. 1137
- 1086 Park, R. J., D. J. Jacob, B. D. Field, R. M. Yantosca, and M. Chin (2004), 1138
 1087 Natural and transboundary pollution influences on sulfate-nitrate-ammonium 1139
 1088 aerosols in the United States: Implications for policy, *J. Geophys. 1140
 1089 Res.*, *109*, D15204, doi:10.1029/2003JD004473. 1141
- 1090 Park, R. J., et al. (2005), Export efficiency of black carbon aerosol in 1142
 1091 continental outflow: Global implications, *J. Geophys. Res.*, *110*, 1143
 1092 D11205, doi:10.1029/2004JD005432. 1144
- 1093 Parrish, D. D., M. Trainer, D. Hereld, E. J. Williams, K. J. Olszyna, R. A. 1145
 1094 Harley, J. F. Meagher, and F. C. Fehsenfeld (2002), Decadal change in 1146
 1095 carbon monoxide to nitrogen oxide ratio in the U.S. vehicular emissions, 1147
 1096 *J. Geophys. Res.*, *107*(D12), 4140, doi:10.1029/2001JD000720. 1148
- 1097 Penner, J. E., C. S. Atherton, J. Dignon, S. J. Ghan, J. J. Walton, and 1149
 1098 S. Hameed (1991), Tropospheric nitrogen: A three-dimensional study of 1150
 1099 sources, distributions, and deposition, *J. Geophys. Res.*, *96*, 959–990. 1151
- 1100 Pickering, K. E., Y. S. Wang, W. K. Tao, C. Price, and J. F. Muller (1998), 1152
 1101 Vertical distributions of lightning NO_x for use in regional and global 1153
 1102 chemical transport models, *J. Geophys. Res.*, *103*, 31,203–31,216. 1154
- 1103 Prather, M. J., et al. (2001), Atmospheric chemistry and greenhouse gases, 1155
 1104 in *Climate Change 2001: The Scientific Basis*, edited by J. T. Houghton 1156
 1105 et al., pp. 239–287, Cambridge Univ. Press, New York. 1157
- 1106 Price, C., and D. Rind (1992), A simple lightning parameterization for 1158
 1107 calculating global lightning distributions, *J. Geophys. Res.*, *97*, 9919– 1159
 1108 9933. 1160
- 1109 Price, C., J. Penner, and M. Prather (1997), NO_x from lightning: 1. Global 1161
 1110 distribution based on lightning physics, *J. Geophys. Res.*, *102*, 5929– 1162
 1111 5941. 1163
- 1112 Richter, A., and J. P. Burrows (2002), Tropospheric NO₂ from GOME 1164
 1113 measurements, *Adv. Space Res.*, *29*, 1673–1683. 1165
- 1114 Richter, A., and T. Wagner (2001), Diffuser plate spectral structures and 1166
 1115 their influence on GOME slant columns, technical note, 4 pp., Univ. of 1167
 1116 Bremen, Bremen, Germany. 1168
- 1117 Richter, A., V. Eyring, J. P. Burrows, H. Bovensmann, A. Lauer, B. Sierk, 1169
 1118 and P. J. Crutzen (2004), Satellite measurements of NO₂ from interna- 1170
 1119 tional shipping emissions, *Geophys. Res. Lett.*, *31*, L23110, doi:10.1029/ 1171
 1120 2004GL020822. 1172
- 1121 Richter, A., J. P. Burrows, H. Nüß, C. Granier, and U. Niemeier (2005), 1173
 1122 Significant increase in tropospheric nitrogen dioxide over China observed 1174
 1123 from space, *Nature*, *437*, 129–132, doi:10.1038/nature04092. 1175
- Rothman, L. S., et al. (1998), The HITRAN molecular spectroscopic data- 1124
 base and HAWKS (HITRAN atmospheric workstation): 1996 edition, 1125
J. Quant. Spectrosc. Radiat. Transfer, *60*, 665–710. 1126
- Ryerson, T. B., et al. (2003), Effect of petrochemical industrial emissions of 1127
 reactive alkenes and NO_x on tropospheric ozone formation in Houston, 1128
 Texas, *J. Geophys. Res.*, *108*(D8), 4249, doi:10.1029/2002JD003070. 1129
- Spurr, R. J. D. (2002), Simultaneous derivation of intensities and weighting 1130
 functions in a general pseudo-spherical discrete ordinate radiative transfer 1131
 treatment, *J. Quant. Spectrosc. Radiat. Transfer*, *75*, 129–175. 1132
- Spurr, R. J. D., T. P. Kurosu, and K. V. Chance (2001), A linearized discrete 1133
 ordinate radiative transfer model for atmospheric remote sensing 1134
 retrieval, *J. Quant. Spectrosc. Radiat. Transfer*, *68*, 689–735. 1135
- Streets, D., et al. (2003), An inventory of gaseous and primary aerosol 1136
 emissions in Asia in the year 2000, *J. Geophys. Res.*, *108*(D21), 8809, 1137
 doi:10.1029/2002JD003093. 1138
- Thornton, J. A., P. J. Wooldridge, and R. C. Cohen (2000), Atmospheric 1139
 NO₂: In situ laser-induced fluorescence detection at parts per trillion 1140
 mixing ratios, *Anal. Chem.*, *72*, 528–539. 1141
- van Noije, T. P. C., et al. (2006), Multi-model ensemble simulations of 1142
 tropospheric NO₂ compared with GOME retrievals for the year 2000, 1143
Am. Chem. Phys. Discuss., *6*, 2965–3047. 1144
- Wang, Y., D. J. Jacob, and J. A. Logan (1998), Global simulation of tropo- 1145
 spheric O₃ - NO_x - hydrocarbon chemistry: 1. Model formulation, 1146
J. Geophys. Res., *103*, 10,713–10,726. 1147
- Wang, Y. X., M. B. McElroy, T. Wang, and P. I. Palmer (2004), Asian 1148
 emissions of CO and NO_x: Constraints from aircraft and Chinese station 1149
 data, *J. Geophys. Res.*, *109*, D24304, doi:10.1029/2004JD005250. 1150
- Wild, O., M. J. Prather, and H. Akimoto (2001), Indirect long-term 1151
 global cooling from NO_x emissions, *Geophys. Res. Lett.*, *28*, 1719– 1152
 1722. 1153
- Yienger, J. J., and H. Levy (1995), Empirical model of global soil-biogenic 1154
 NO_x emissions, *J. Geophys. Res.*, *100*, 11,447–11,464. 1155
- T. H. Bertram, R. C. Cohen, and P. J. Wooldridge, Department of 1157
 Chemistry, University of California, Berkeley, Berkeley, CA 94720-1640, 1158
 USA. (tbertram@berkeley.edu; cohen@cchem.berkeley.edu; pjwool@ 1159
 socrates.berkeley.edu) 1160
- K. Chance and C. E. Sioris, Harvard-Smithsonian Center for Astro- 1161
 physics, Cambridge, MA 02138-1516, USA. (kchance@cfa.harvard.edu; 1162
 csioris@cfa.harvard.edu) 1163
- F. M. Flocke, Atmospheric Chemistry Division, National Center for 1164
 Atmospheric Research, Boulder, CO 80307, USA. (ffl@ucar.edu) 1165
- R. V. Martin, Department of Physics and Atmospheric Science, 1166
 Dalhousie University, Halifax, NS B3H 3J5, Canada. (randall.martin@ 1167
 dal.ca) 1168
- J. A. Neuman, T. B. Ryerson, and A. Swanson, Chemical Sciences 1169
 Division, Earth System Research Laboratory, NOAA, Boulder, CO 80307, 1170
 USA. (andy.neuman@noaa.gov; thomas.b.ryerson@noaa.gov) 1171